Characterization of the Ni(II) Phase Formed on Silica Upon Deposition−Precipitation

Paolo Burattin,[†] Michel Che,[‡] and Catherine Louis*

Laboratoire de Réactivité de Surface, URA 1106 CNRS, Université P. et M. Curie, 4 place Jussieu, 75252 Paris Cedex 05, France

Received: January 13, 1997; In Final Form: June 11, 1997[⊗]

The nature of the Ni(II) phase formed on silica during the preparation by deposition−precipitation (DP) of Ni/SiO_2 samples is shown to depend on the silica surface area and the time of deposition−precipitation. Ni/SiO_2 samples have been characterized by XRD, IR, EXAFS, TPR, TEM, STEM-EDX, and BET. With silica of low surface area and for short DP time (≤4 h), the Ni(II) phase is mainly a turbostratic nickel hydroxide with a small amount of 1:1 nickel phyllosilicate. With silica of high surface area and for short DP time (≤100 min), the Ni(II) phase is mainly a 1:1 nickel phyllosilicate. For longer DP time (>4 h) and with both types of silica, the Ni(II) phase is an ill-crystallized 1:1 nickel phyllosilicate. However, the latter is better crystallized with silica of low surface area. Almost the same Ni(II) phases were obtained whether silica was porous or not. However, the Ni(II) phase is better crystallized and the interface with the support is larger with nonporous silica than with porous one.

Introduction

Silica-supported metal or metal oxide catalysts have been and are still extensively studied in academic research because silica support is considered as inert, i.e., as a mere dispersant of the active phase. However, several authors have revealed that silica is not so inert and may react with the metal precursors and form silicates during catalyst preparation. Their formation depends on the reactivity of silicic species with metal complexes. The formation of Ni silicate,[1−8] Co silicate,[9] Cu silicate,[10,11] Ce silicate,[12] and Zn silicate[13] has been reported or postulated during the preparation of silica-supported catalysts by impregnation or cation exchange. The case of the formation of nickel silicate during catalyst preparation is the most known.[1−8] To our knowledge, Houalla et al.[1] were the first authors to show that nickel silicates are formed during the so-called cation exchange preparation. More recently, Che et al.[4,6,8] have confirmed the formation of nickel phyllosilicates (layered nickel silicates) by EXAFS and IR. They are formed either during "exchange" at pH = 8.3 or after "exchange" at pH = 9.8 during the washing step, i.e., when the Ni(II) complex is not a complex hexaammine but contains some water ligands, which enable oxolation-type condensation reaction with silicic species in solution, arising from silica dissolution at basic pH.[6] Formation of nickel phyllosilicates was also observed in impregnated samples, but in very small proportion.[7] They are formed during the drying step.

The method of deposition−precipitation, developed by Geus et al.,[14−16] is also a preparation method, which leads to the formation of supported metal silicate. The preparation of Ni/SiO_2 catalysts was the most studied. This method derives from precipitation methods,[17−19] and consists of the precipitation of a nickel(II) phase onto silica support by basification of a nickel salt solution containing silica in suspension. The key factor of this preparation is the basification, i.e., the gradual and homogeneous addition of hydroxide ions throughout the whole solution, in order to locally avoid high pH, and the precipitation of nickel hydroxide in solution. The use of urea ($CO(NH_2)_2$) rather than sodium hydroxide is advised because solution mixing and basification can be performed in two separate steps: urea is mixed to the solution at room temperature, and urea hydrolysis starts when the mixture is heated at 90 °C: hydroxide ions are homogeneously generated within the solution:

$$CO(NH_2)_2 + 3H_2O \rightarrow 2NH_4^+ + HCO_3^- + OH^- \quad \text{(I)}$$

Isocyanate ions are the intermediate species formed during urea hydrolysis and is the limiting step of the reaction:[20]

$$CO(NH_2)_2 \rightarrow NH_4^+ + OCN^- \quad \text{(II)}$$

Characterization studies have shown that nickel precipitates on silica as layered nickel silicate whereas the precipitation of nickel hydroxide was a priori expected.[15,16,21−23] Van Dillen et al.[15] have suggested that the formation of nickel antigorite (structural formula $Si_2Ni_3O_5(OH)_4$), also called 1:1 nickel phyllosilicate (see below). This hypothesis was then strengthened by characterization studies of XRD, XPS, TPR, BET, electron microscopy,[22−25] and then of EXAFS and IR.[5,8]

Catalysts prepared by this method exhibit many advantages compared to more conventional ones: it is possible to obtain high nickel loadings (>20 wt %) depending on the time of deposition−precipitation. After catalyst reduction, small metal particles are obtained with rather narrow size distribution.[25−31] The same results are obtained with adsorption or exchange techniques, but the metal loading rarely exceeds 5%. In contrast, with impregnation techniques, it is easy to obtain high metal loading, but the size distribution of metal particles is usually broad, and the mean particle size is large. The metal particles of samples prepared by deposition−precipitation do not easily sinter because of the strong interaction with the support.[22−25,27−31] In addition, this preparation method is highly reproducible.[26] Because of these numerous advantages, this method was for example, chosen for the preparation of the standard nickel/silica catalyst EuroNi-1.[22,23,32]

Most of the deposited−precipitated Ni/SiO_2 catalysts referenced in the literature[5,16,22,24,26,27] were prepared with silica of high surface area (≥200 $m^2 \cdot g^{-1}$), and exhibit high Ni loadings, which require several hours of deposition−precipitation. The

* Corresponding author. E-mail: louisc@ccr.jussieu.fr.
[†] Permanent address: Rhône Poulenc CRIT-Carrières, 86 avenue des Frères Perret, BP 62, 69192 Saint Fons Cedex, France
[‡] Member of the Institut Universitaire de France.
[⊗] Abstract published in *Advance ACS Abstracts,* August 1, 1997.

S1089-5647(97)00194-6 CCC: $14.00

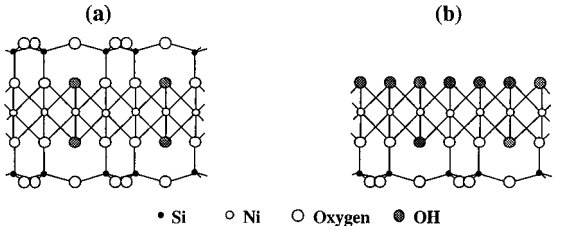

Figure 1. Projection on the *bc* plane of (a) a layer of 1:1 nickel phyllosilicate; (b) a layer of 2:1 nickel phyllosilicate, from refs 64 and 65. Reproduced with permission from ref 65. Copyright 1970 [Elsevier].

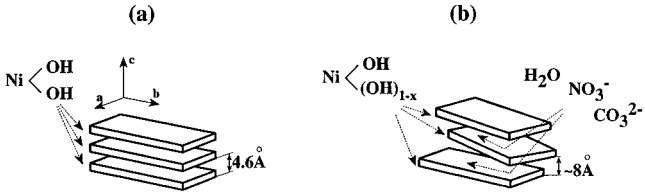

Figure 2. Structure of nickel hydroxide: (a) β-$Ni(OH)_2$; (b) α-$Ni(OH)_2$, from ref 37. Reproduced with permission from ref 37. Copyright 1991 [CDR].

influence of the DP time, the silica surface area, and the silica porosity on the nature of the deposited−precipitated Ni(II) phase has not been systematically studied; this is the goal of the present paper. This should help to better understand the role of silica as reactant, and the chemical mechanisms occurring during deposition−precipitation, which lead to the formation of nickel phyllosilicates; this will be the scope of a forthcoming paper.[33]

Structure of Nickel Phyllosilicates and Hydroxides

There are two types of layered nickel silicates:

1. 2:1 nickel phyllosilicate whose structural formula is $Si_4Ni_3O_{10}(OH)_2$ when it is well-crystallized; it is also called Ni-talc or willemseite (Figure 1a):

2. 1:1 nickel phyllosilicate or serpentine ($Si_2Ni_3O_5(OH)_4$), also called Ni-lizardite or nepouite when the layers are planar (Figure 1b), Ni-antigorite when the layers are splintery, and Ni-chrysotile when they are curled into cylindrical rolls.

These structures are well-known and have been extensively described in the literature.[34] A layer of 1:1 nickel phyllosilicate consists of a brucite-type sheet containing Ni(II) in octahedral coordination and a sheet containing linked tetrahedral SiO_4 units (Figure 1b). In 2:1 nickel phyllosilicates, two sheets of linked SiO_4 units sandwich the brucite-type sheets (Figure 1a). The layers of 1:1 nickel phyllosilicate are neutral and do not exhibit ion-exchange properties; those in 2:1 phyllosilicate can be negatively charged when it is low-crystallized, because of octahedral cation vacancies (stevensite, $Si_4Ni_{3-x}O_{10}(OH)_2M(I)_{2x}$).[35] In this case, the electric charge is balanced by the presence of cations in the interlayers.

$Ni(OH)_2$ is also a layered compound consisting of brucitic layers of octahedral Ni(II) with structural OH groups. Depending on the layer stacking, two types of structures may be formed (Figure 2):

1. β-$Ni(OH)_2$ exhibits a tridimensional structure consisting of stacked brucitic-like layers (00*l* plane) with a *d*(001) basal spacing equal to 4.6 Å[36] (Figure 2a);

2. α-$Ni(OH)_2$, also called turbostratic nickel hydroxide, exhibits a bidimensional structure because of the disordered stacking of the brucitic layers, which are separated by intercalated anionic species (Figure 2b). The basal spacing depends on the nature of intercalated anions (nitrates, carbonates: *d*(001) ≈8 Å; acetates: *d*(001) ≈9 Å)[37], which ensure the electron neutrality of the nonstoichiometric layers ($Ni(OH)_{2-x}$).[37]

TABLE 1: Change in the Ni Loading and Yield of the Ni(II) Phase Formed as a Function of the DP Time

	Ni/XOA 400		Ni/XO30LS	
DP time	wt % Ni	yield (%)	wt % Ni	yield (%)
70 min	5.2	11.4	2.8	6.1
2.5 h	17.2	37.8	12.5	27.5
4 h	25.1	55.1	21.3	46.8
8 h	35.8	78.7	31.2	68.6
16 h	44.6	98.0	40.8	89.7
24 h	45.4	99.8	42.1	92.5
50 h	44.2	97.1	42.8	94.0
100 h	42.8	94.0	45.4	99.8

Experimental Section

1. Sample Preparation. The Ni/SiO_2 samples were prepared according to the deposition−precipitation method described by Hermans and Geus:[16] 380 mg of silica was put into a vessel thermostated at 90 °C. 50 mL of an aqueous solution containing nickel nitrate (0.14 M), urea (0.42 M), and nitric acid (0.02 M) was added at $t = 0$, and the suspension was magnetically stirred. Nitric acid allows to better follow the changes in pH during basification.[15,16,33] The atomic ratio Ni:Si was equal to 1.1 in the suspension. The solution reached 90 °C within 3 min, and the deposition−precipitation started. After a given time of deposition−precipitation, the suspension was cooled to 20−25 °C and then filtered. Cooling the mixture to 25 °C is crucial to solubilize nickel bicarbonate formed on silica during deposition−precipitation; this point will be developed in section 3.d. Then, the sample was washed three times: after addition of 20 mL of distilled water, the mixture was stirred during 10 min at 50−60 °C before filtration. Finally, the sample was dried at 90 °C for 24 h.

Most of the samples were prepared with porous Spherosil silicas (Rhône Poulenc, France, purity > 99.5%): XOA400 ($S_{BET} = 356\ m^2 \cdot g^{-1}$, pore volume = $1.25\ cm^3 \cdot g^{-1}$, average pore diameter ≈80 Å) and XO30LS ($S_{BET} = 44\ m^2 \cdot g^{-1}$, pore volume = $2.27\ cm^3 \cdot g^{-1}$, average pore diameter ≈1000 Å). The samples are hereafter referred to as Ni/XOA400(t) and Ni/XO30LS(t), respectively; *t* is the time of deposition−precipitation. A few samples were also prepared with nonporous Aerosil silicas (Degussa, Germany, purity > 99.95%): AD380 ($S_{BET} = 380\ m^2 \cdot g^{-1}$) and OX50 ($S_{BET} = 50\ m^2 \cdot g^{-1}$).

Nickel nitrate ($Ni(NO_3)_2 \cdot 6H_2O$) was provided by Aldrich (purity > 99.0%). Basic nickel carbonate $NiCO_3 \cdot 2Ni(OH)_2 \cdot 4H_2O$ used as a reference sample (see section 1 of results) was supplied by Fluka.

Chemical analyses were performed by inductive coupling plasma in the CNRS Center of Chemical Analysis (Vernaison, France). In the following, the Ni weight loading of the samples is expressed in wt % of Ni per g of sample calcined in air at 1000 °C:

$$\text{wt \% Ni} = (M_{Ni})/(M_{NiO} + M_{SiO_2}) \times 100$$

The yield of deposition−precipitation is defined as follows: yield (%) = (wt % Ni)/(wt % Ni(∞)) × 100, where wt % Ni(∞) is the maximum Ni loading when all the Ni in solution has precipitated; it is equal to 45.5 wt %.

The changes in the Ni loading and yield of deposition−precipitation versus the time of deposition−precipitation are presented in Table 1.

To get reference samples for the characterization of the Ni/SiO_2 samples, two sets of bulk 2:1 and 1:1 nickel phyllosilicates, synthesized and aged during 15 days at 25 °C (ill-crystallized) and 150 °C (better-crystallized) have been prepared by Decar-

TABLE 2: Fitted Structural Parameters of the 2:1 Nickel Phyllosilicate Synthesized at 500 °C, Determined by EXAFS at the Ni K-Edge for the Second Shell

neighbors	N	R (Å)	γ (Å^{-2})	σ (Å)[a]	ΔE (eV)	fit
Ni	6.0[a]	3.06	1.00[a]	0.082	−0.6[a]	2.0×10^{-3}
Si	4.0[a]	3.25	0.85[a]	0.092	−9.0	

[a] Fixed parameters.

reau (HydrASA, URA 721 CNRS, Université de Poitiers, France) according to a hydrothermal process described elsewhere.[35,38]

Nickel precipitates were prepared in the absence of silica support: 200 mL of an aqueous solution containing nickel nitrate (0.14 M), urea (0.42 M), and nitric acid (0.02 M) were put into a Teflon vessel thermostated at 90 °C and magnetically stirred. After a given time of reaction, the solution was cooled to 25 °C and filtered, and the nickel precipitate was washed and dried according to the procedure described above.

2. Characterization Techniques. The XRD spectra were registered on a Siemens diffractometer (D500) using Cu Kα radiation. The phase identifications were performed by comparison with the tabulated JCPDS *d* spacing files.

The IR spectra were scanned (5 scans) at room temperature with a FTIR Perkin-Elmer 1750 spectrophotometer. The samples were finely ground and dispersed in KBr pellets with a ratio of about 1 mg per 100 mg of KBr. The resolution of the IR spectra is 4 cm^{-1}.

EXAFS measurements at the K absorption edge of Ni were performed at the LURE radiation synchrotron facility (EXAFS I) using the X-ray beam emitted by the DCI storage ring (positron energy 1.85 GeV, ring current 300 mA). The spectra were recorded in transmission mode at room temperature using two air-filled ionization chambers. The energy was scanned with 2 eV steps from 8200 to 9200 eV (K absorption edge of Ni: 8331 eV), using a channel-cut single crystal of silicon as monochromator. EXAFS measurements were carried out three times for each sample. The absorption variation through the edge $\Delta(\mu x)$ was at least 0.5. The analyses of the EXAFS spectra were performed following standard procedures for background removal, extraction of the EXAFS signal, and normalization (Lengeler−Eisenberger method) to the edge absorption. Fourier transforms were obtained after multiplication of the EXAFS signal by a factor k^3, using the same Kaiser window for the references and the investigated systems. Data treatment was performed with the software EXAFS pour le Mac.[39] The amplitude and phase functions for Ni−O and Ni−Ni pairs were experimentally obtained from the spectra of NiO and β-Ni(OH)$_2$, respectively, and those for Ni−Si pairs from the McKale files. γ_{Si} has been found equal to 0.85 when calibrated with a well-crystallized 2:1 nickel phyllosilicate synthesized at 500 °C, assuming that $N_{Ni} = 6$, $N_{Si} = 4$, $\gamma_{Ni} = 1$, and $\Delta E_{Si} = -0.6$ eV (Table 2).

The samples were reduced by temperature-programmed reduction (TPR) in a quartz gas flow reactor, from room temperature to 900 °C, with a heating rate of 7.5 °C·min^{-1}, under a stream of 5% v/v H_2 in argon (total flow rate 25 mL·min^{-1}) at atmospheric pressure. The intensities of the TPR profiles are expressed in arbitrary units. However, the same sample weight (40 mg) and the same attenuation of the thermal conductivity detector were used, except for the TPR profiles of Figure 18.

The Ni/SiO$_2$ samples were observed by TEM with a JEOL JEM 100CXII microscope equipped with a top-entry device and operating at 100 kV. Some samples were also studied by STEM-EDX using a JEOL JEM 100CXII microscope equipped with a scanning device ASID 4D and a Si(Li) energy-dispersive spectrometer with a Link AN10000 X-ray analyzer.

The BET surface area measurements were performed with a Quantasorb Junior apparatus.

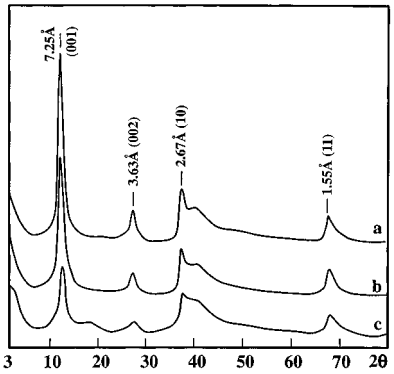

Figure 3. XRD pattern of nickel precipitates obtained in the absence of silica after different times of precipitation: (a) 2.5 h (sample 1); (b) 4 h (sample 2); (c) 16 h (sample 3).

TABLE 3: Nickel Precipitates Prepared in the Absence of Silica

sample	time of preciptn (h)	precipitate formula
1	2.5	$[Ni^{2+}(OH^-)_{1.063}]\,[(CO_3^{2-})_{0.326}(NO_3^-)_{0.066}(NCO^-)_{0.219}]$
2	4	$[Ni^{2+}(OH^-)_{1.146}]\,[(CO_3^{2-})_{0.311}(NO_3^-)_{0.085}(NCO^-)_{0.147}]$
3	16	$[Ni^{2+}(OH^-)_{1.006}]\,[(CO_3^{2-})_{0.448}(NO_3^-)_{0.069}(NCO^-)_{0.029}]$
4	48	$[Ni^{2+}(OH^-)_{0.978}]\,[(CO_3^{2-})_{0.475}(NO_3^-)_{0.053}(NCO^-)_{0.018}]$

Results and Interpretation

1. Characterization of the Nickel Precipitates Prepared in the Absence of Silica. A set of nickel precipitates has been obtained with different precipitation times (Table 3). Samples 1−3 (2.5−16 h of precipitation) exhibit a XRD pattern characteristic of a two-dimensional structure with *hk* and *00l* reflections (Figure 3), characteristic of turbostratic nickel hydroxide, α-Ni(OH)$_2$:[37] the asymmetric lines at 2.67 and 1.55 Å may be attributed to the 10 and 11 reflections, respectively, and the two symmetric ones at 7.25 and 3.63 Å to the 001 and 002 basal reflections, characteristic of a bidimensional structure.[36,37]

The line intensity of the XRD patterns decreases with the time of precipitation (Figure 3), and sample 4 obtained after 48 h is amorphous, indicating that the crystallinity of the Ni(II) precipitate decreases with the time of precipitation.

The IR spectra (Figure 4) are also characteristic of the formation of a turbostratic nickel hydroxide because of the presence of bands of δ_{OH} vibration at 640 cm^{-1} and ν_{NiO} vibration of the hydroxide network at 480 cm^{-1}.[40] The band at 3645 cm^{-1} is attributed to the ν_{OH} vibration and the broad one at 3500 cm^{-1} to intercalated physisorbed water molecules.

The presence of different intercalated anionic species in the Ni(II) precipitates is attested by the existence of (1) a strong band at 2215 cm^{-1} and a sharp one at 1287 cm^{-1}, both due to isocyanate NCO$^-$ ions,[41,42] which arise from urea decomposition (eq II). It may be noted that the isocyanate band at 2215 cm^{-1} splits into two bands at 2225 and 2205 cm^{-1} during precipitation; (2) bands at 1610, 1460, 1375, 1070, and 833 cm^{-1} due to carbonate ions;[43] they are also observed in the IR spectrum of a commercial basic nickel carbonate $NiCO_3 \cdot 2Ni(OH)_2 \cdot 4H_2O$ (Figure 4d); the shoulder at 1630 cm^{-1} may be attributed to δ_{H2O} vibration;[40] and (3) a band at 1385 cm^{-1} characteristic of nitrate ions.[43]

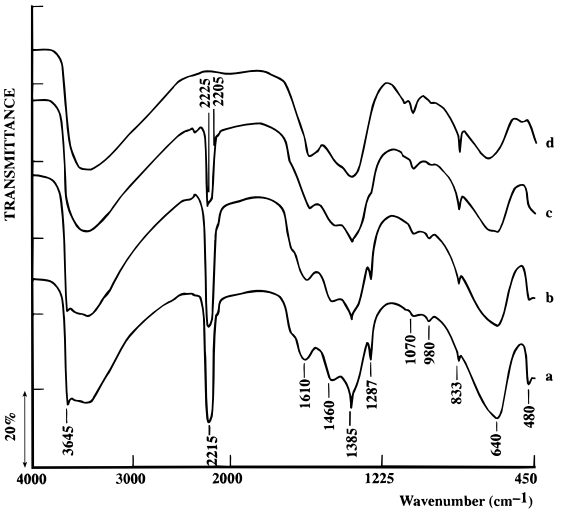

Figure 4. IR spectra of nickel precipitates obtained in the absence of silica after different times of precipitation: (a) 2.5 h (sample 1); (b) 4 h (sample 2); (c) 16 h (sample 3); (d) basic nickel carbonate $Ni(CO_3)_2 \cdot 2Ni(OH)_2 \cdot 4H_2O$.

The IR spectra evolve with the time of precipitation: the nitrate and isocyanate bands decrease while the carbonate bands increase. In addition, the ν_{OH} band at 3645 cm^{-1} decreases, indicating that more OH groups are linked by hydrogen bonds to intercalated water.

The IR spectra show that the precipitated turbostratic nickel hydroxides contain nitrate, carbonate, and isocyanate anions in the interlayer spacing. According to Génin et al.,[37] the brucitic layers are nonstoichiometric to ensure electron neutrality, so that the general structural formula may be proposed: $[Ni^{2+}(OH^-)_{2-x}]\,[(CO_3^{2-})_a(NO_3^-)_b(NCO^-)_c \cdot yH_2O]$. The values for *a*, *b*, *c*, and *x* of the different samples were determined by chemical analysis (Table 3). In agreement with the IR results, the amount of NCO^- was found to decrease and that of CO_3^{2-} to increase with the time of precipitation. It may be noted that after 48 h of precipitation, the formula of sample 4 is very close to that of the basic nickel carbonate $NiCO_3 \cdot Ni(OH)_2$.

The loss of crystallinity with the precipitation time, observed by XRD, is probably related to a phenomenon of dissolution−reprecipitation (dissolution of the precipitated nickel hydroxide and reprecipitation of basic nickel carbonate). The frequency change of the NCO^- vibration band at about 2215 cm^{-1} is probably due to the change in the anion environment when the nickel hydroxide transforms into basic nickel carbonate.

2. Characterization of Nickel Phyllosilicates Prepared by Hydrothermal Process. *a. X-ray Diffraction.* The XRD patterns of 1:1 and 2:1 nickel phyllosilicates synthesized at 25 and 150 °C are shown in Figure 5. The line assignment (Figure 5) is based on published results.[44−46] As for the turbostratic nickel hydroxide (Figure 3), the nickel phyllosilicates exhibit a XRD pattern characteristic of a two-dimensional structure with *hk* bands and *00l* lines. It may be noted that the main difference between nickel hydroxide and nickel phyllosilicates XRD patterns (Figures 3 and 5) is the presence of an additional 02-11 reflection at ≈4.5 Å for the nickel phyllosilicates. In addition, the 001 line is thinner for nickel hydroxides (Figure 3) than for nickel phyllosilicates (Figure 5), even when nickel hydroxides exhibit low crystallinity. Furthermore, the position and width of the 001 line do not depend on the crystallinity, in contrast with nickel phyllosilicates (Figure 5) whose 001 line width and basal spacing decrease when the synthesis temperature, i.e., the crystallinity, increases.[44,45] The *d*(001) spacing also depends on the nature of the phyllosilicate. In agreement

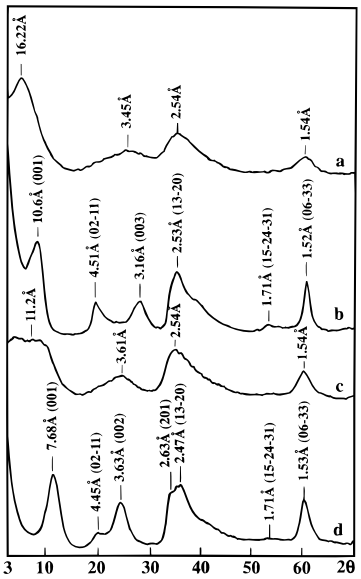

Figure 5. XRD pattern of (a) 2:1 nickel phyllosilicate synthesized at 25 °C; (b) 2:1 nickel phyllosilicate synthesized at 150 °C; (c) 1:1 nickel phyllosilicate synthesized at 25 °C; (d) 1:1 nickel phyllosilicate synthesized at 150 °C.

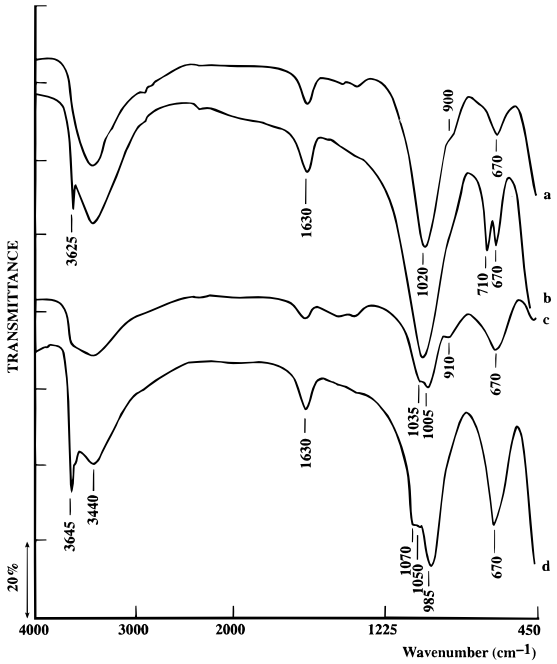

Figure 6. IR spectra of bulk nickel phyllosilicates: (a) 2:1 nickel phyllosilicate synthesized at 25 °C; (b) 2:1 nickel phyllosilicate synthesized at 150 °C; (c) 1:1 nickel phyllosilicate synthesized at 25 °C; (d) 1:1 nickel phyllosilicate synthesized at 150 °C.

with previous works,[44−46] it varies between 16 and 11 Å for 2:1 nickel phyllosilicate (Figure 5a,b) and between 11 and 8 Å for 1:1 nickel phyllosilicate (Figure 5c,d) for temperature of synthesis between 25 and 150 °C.

b. IR Spectroscopy. Figure 6 exhibits the IR spectra and band positions of 2:1 and 1:1 nickel phyllosilicates, synthesized at 25 °C (ill-crystallized) and 150 °C (better-crystallized). In agreement with previous works,[8,44] the IR spectra depend on the nickel phyllosilicate crystallinity. For nickel phyllosilicates synthesized at 25 °C, the presence of water molecules intercalated between the layers[45] inhibits the observation of the ν_{OH} vibration band at ≈3640 cm^{-1}; only a broad band at ≈3440 cm^{-1} is observed in the OH stretching frequency range. When the temperature of hydrothermal synthesis reaches 150 °C, the

TABLE 4: Intensity Ratio of the Bands $I_{670\ cm^{-1}}/I_{1000\ cm^{-1}}$ in Bulk Nickel Phyllosilicates

samples		$I_{670\ cm^{-1}}/I_{1000\ cm^{-1}}$	Figure
2:1 phyllosilicate	25 °C	0.23	6a
	150 °C	0.34	6b
1:1 phyllosilicate	25 °C	0.58	6c
	150 °C	0.52	6d

stretching ν_{OH} band is observed at 3625 and 3645 cm^{-1} for 2:1 and 1:1 nickel phyllosilicates, respectively (Figure 6b,d). In the δ_{OH} range, both types of silicate synthesized at 25 °C exhibit a broad band at about 670 cm^{-1} (Figure 6a,c). The 1:1 nickel phyllosilicate exhibits the same δ_{OH} band when it is synthesized at 150 °C (Figure 6d) whereas the 2:1 nickel phyllosilicate exhibits a doublet at 710 and 670 cm^{-1} (Figure 6b). The band at 710 cm^{-1} has already been assigned to the δ_{OH} vibration of isolated OH surrounded by three Ni atoms, whereas that at 670 cm^{-1} was assigned to a tetrahedral SiO mode.[8,47]

For 1:1 nickel phyllosilicate synthesized at 25 °C (Figure 6c), the SiO stretching vibration provides two bands at 1005 and ≈1035 cm^{-1}. In agreement with previous work,[8] the band at 1005 cm^{-1} shifts toward lower wavenumber, to 985 cm^{-1}, when the synthesis temperature increases up to 150 °C (Figure 6d) whereas the shoulder at 1035 cm^{-1} shifts toward higher wavenumber and splits into two bands at 1050 and 1070 cm^{-1}. For 2:1 nickel phyllosilicate, the SiO stretching band is at about 1020 cm^{-1} and is independent of the synthesis temperature (Figure 6a,b). It may be noted that the IR spectra of nickel phyllosilicates synthesized at 25 °C exhibit a shoulder at 900−910 cm^{-1} (Figure 6a,c). According to Decarreau et al.,[48] nickel phyllosilicates synthesized at low-temperature possess a high proportion of layer edges, and therefore a lot of Si−OH groups because of the ill-crystallinity. These Si−OH groups are responsible for the Si−O stretching vibration band at about 920 cm^{-1}.[49]

Hence, ill-crystallized 1:1 and 2:1 nickel phyllosilicates (synthesized at 25 °C) cannot be distinguished from their δ_{OH} vibration mode which are very close (≈670 cm^{-1}). However, they can be distinguished from their different SiO stretching vibration frequencies at 1035 and 1005 cm^{-1} for 1:1 nickel phyllosilicate and 1020 cm^{-1} for 2:1 nickel phyllosilicate (Figure 6). In addition, as indicated by Decarreau,[50] the intensity ratio of the bands δ_{OH}/ν_{SiO}, i.e., $I_{670\ cm^{-1}}/I_{1000\ cm^{-1}}$ in 1:1 nickel phyllosilicate is about twice that in 2:1 nickel phyllosilicate (Table 4).

On the other hand, turbostratic nickel hydroxide, α-$Ni(OH)_2$, may be discriminated from nickel phyllosilicates by the absence of SiO streching vibration band at 1000−1040 cm^{-1} and by the different δ_{OH} frequencies: 640 cm^{-1} for α-$Ni(OH)_2$ and 670 cm^{-1} for ill-crystallized nickel phyllosilicates.

c. Temperature-Programmed Reduction. The Ni(II) precipitate obtained in the absence of silica (Figure 7a) is more easily reducible than the nickel phyllosilicates (Figure 7b−e), as attested by its lower temperature peak (320 °C). For a given temperature synthesis, 2:1 nickel phyllosilicate is reduced at higher temperature than 1:1 nickel phyllosilicate (Figure 7), in agreement with previous results.[51] In addition, the reducibility of nickel phyllosilicates decreases when the crystallinity, i.e., the temperature of hydrothermal synthesis, increases (Figure 7), in agreement with Carriat et al.[51,52]

3. Characterization of the Nickel(II) Phase Deposited−Precipitated on Porous Silicas. Table 1 shows that the Ni loading increases versus the DP time and reaches a plateau beyond 16 h. This plateau corresponds to an aging period since almost all the Ni is already precipitated. The Ni loading evolves almost in the same way for both types of silica. The changes

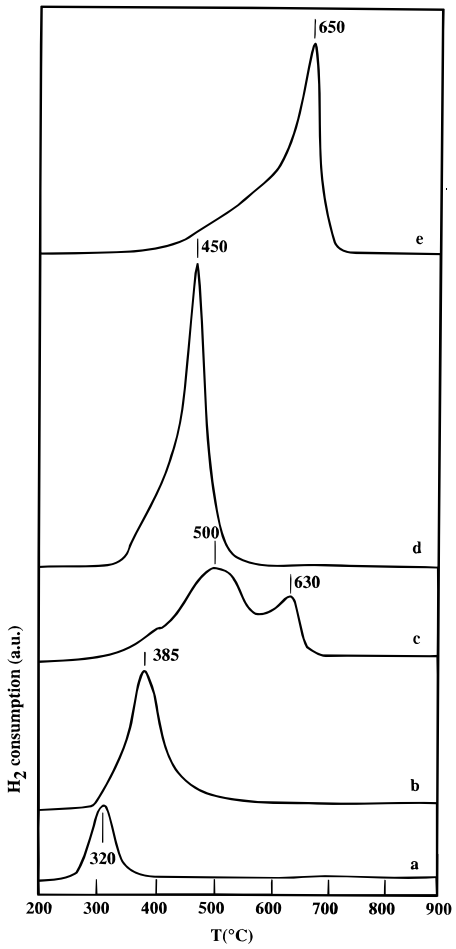

Figure 7. TPR profile of bulk compounds: (a) nickel precipitates obtained in the absence of silica; samples 1−4 give the same profile; (b) 1:1 nickel phyllosilicate synthesized at 25 °C; (c) 1:1 nickel phyllosilicate synthesized at 150 °C; (d) 2:1 nickel phyllosilicate synthesized at 25 °C; (e) 2:1 nickel phyllosilicate synthesized at 150 °C.

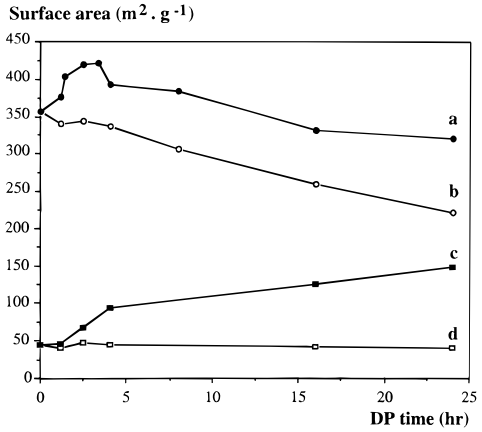

Figure 8. BET surface area of (a) Ni/XOA400; (b) silica XOA400; (c) Ni/XO30LS; (d) silica XO30LS; as a function of the time of deposition-precipitation.

in surface area of the Ni/XOA400 and Ni/XO30LS samples versus the DP time are reported in Figure 8a,c, and compared to those of silicas XOA400 and XO30LS submitted to the same DP treatment, but without nickel nitrate (Figure 8b,d). The changes in surface area will be described and discussed later in section 3f. However, it may be already noted that both the curves of Ni/XOA400 and Ni/XO30LS samples exhibit a break after about 4 h of DP, indicating a change in the process of deposition−precipitation. In the following characterization

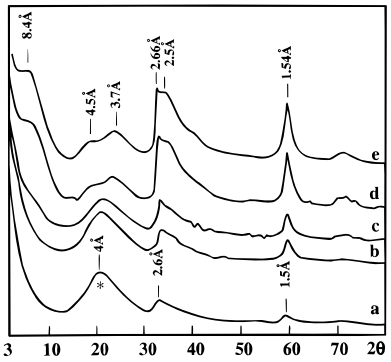

Figure 9. XRD patterns of Ni/XOA400 samples after different times of deposition−precipitation: (a) 70 min; (b) 2.5 h; (c) 4 h; (d) 50 h; (e) 100 h (*, silica).

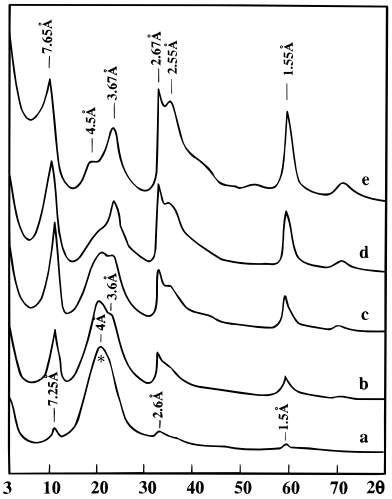

Figure 10. XRD patterns of Ni/XO30LS samples after different times of deposition−precipitation: (a) 70 min; (b) 2.5 h; (c) 4 h; (d) 16 h; (e) 50 h (*, silica).

study, samples prepared during short DP times (≤4 h) will be distinguished from samples prepared during long DP times (>4 h).

a. X-ray Diffraction. The XRD patterns obtained for the Ni/XOA400 samples after different times of deposition−precipitation are shown in Figure 9. For short DP times (≤4 h), the XRD patterns (Figure 9a−c) exhibit a broad band at ≈4 Å, characteristic of amorphous silica, and two asymmetric bands at 2.6 and 1.5 Å. By comparison with the XRD patterns of Figures 3 and 5, the last two bands may be attributed either to the 10 and 11 reflections of a turbostratic nickel hydroxide, or to the 13-20 and 06-33 reflections of ill-crystallized 1:1 or 2:1 nickel phyllosilicates. The 001 line of nickel hydroxide or nickel phyllosilicate expected between 7 and 10 Å is not visible.

For long DP time (≥50 h) (Figure 9d,e), i.e., during the aging period, the broad band of amorphous silica at about 4 Å disappears, and the XRD pattern is better resolved. Three new lines are visible at about 8.4, 4.5, and 3.7 Å. Again, by comparison with the XRD patterns of Figures 3 and 5, they may be attributed to the 001, 02-11 and 002 reflections of an ill-crystallized 1:1 nickel phyllosilicate whose crystallinity slightly improves with time. These XRD results cannot rule out the possible coexistence of 2:1 nickel phyllosilicate or nickel hydroxide.

The XRD patterns of the Ni/XO30LS samples prepared for different times of deposition−precipitation are given in Figure 10. They exhibit a better resolution than those of the Ni/XOA400 samples (Figure 9) even for short DP time; that indicates that the DP Ni(II) phase is better crystallized on silica XO30LS than on silica XOA400. For short DP time (≤4 h) (Figure 10a−c), a line at 7.25 Å grows up as well as a shoulder at ≈3.6 Å on the broad band of silica (≈4 Å). For long DP time (Figure 10d,e), the silica band disappears, and a line at 4.5 Å appears while that at 3.6 Å continues to increase and that at 7.25 Å shifts toward 7.65 Å.

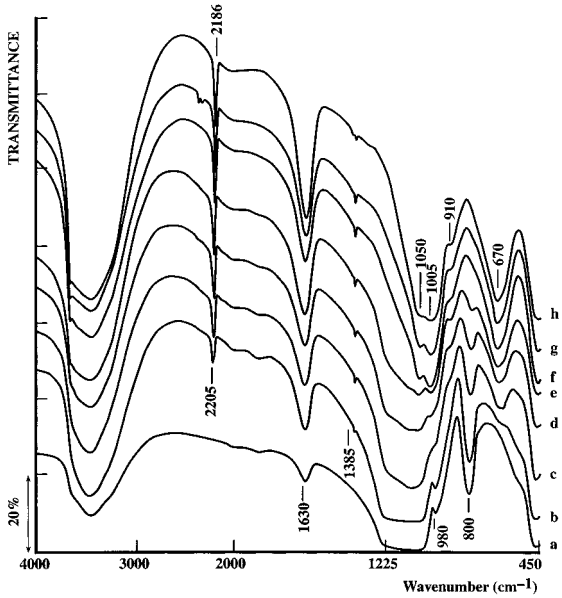

Figure 11. IR spectra of Ni/XOA400 samples after different times of deposition−precipitation: (a) $t = 0$; (b) 70 min; (c) 2.5 h; (d) 4 h; (e) 8 h; (f) 16 h; (g) 24 h; (h) 50 hr.

The narrow line at ≈7.25 Å observed for DP time ≤4 h (Figure 10a−c) cannot be attributed to the 001 reflection of 1:1 nickel phyllosilicate but to that of a turbostratic nickel hydroxide, like in the case of the Ni(II) precipitates prepared in the absence of silica (Figure 3). Indeed, (i) the 001 line of nickel phyllosilicates (Figure 5) is broader than that of hydroxides (Figure 3); (ii) the *d*(001) spacing of nickel phyllosilicates is larger (Figure 5); (iii) the growth of the line at 7.25 Å is not associated to that of the lines at 3.6 and 4.5 Å. The attribution of the 001 line to a turbostratic nickel hydroxide is strengthened by the fact that when HNO_3 is replaced by CH_3COOH in the starting solution of deposition−precipitation, a larger basal spacing is obtained after 4 h of DP: 7.63 instead of 7.25 Å. The change in the basal spacing with the nature of anion is characteristic of a turbostratic nickel hydroxide.[37] Such kind of change cannot succeed in 1:1 nickel phyllosilicates, since there are no intercalated anions because of the neutral layers.[34] However, it is not possible to totally exclude the coexistence of small amounts of nickel phyllosilicates.

For longer DP times, the increasing intensity of the 001 line with the shift toward 7.65 Å (Figure 10d−e) is accompanied by the growth of lines at 4.5, 3.67, 2.67, and 2.55 Å, which may be attributed to the 02-11, 002, 201, and 13-20 reflections of 1:1 nickel phyllosilicate, respectively, by comparison with the pattern in Figure 5d. In addition, the broad band of amorphous silica at about 4 Å disappears. It may be noted that the XRD pattern of Ni/XO30LS (50 h) (Figure 10e) exhibits thinner lines than that of Ni/XOA400 (50 h) (Figure 9d), indicating that 1:1 nickel phyllosilicate in Ni/XO30LS (50 h) is better crystallized than in Ni/XOA400 (50 h).

b. IR Spectroscopy. The IR spectra of the Ni/XOA400 samples are shown in Figure 11. The main changes observed with DP time are the following:

1. The weak asymmetric ν_{Si-OH} vibration band of silica at 980 cm^{-1} disappears beyond 2.5 h of DP (Figure 11c).

2. The symmetric ν_{SiO} vibration band at 800 cm^{-1} and the broad asymmetric one at about 1100 cm^{-1}, characteristic of the silicic network, drastically decrease and disappear beyond 16 h of DP (Figure 11f).

3. A shoulder at about 650 cm^{-1} is observed after 70 min of DP (Figure 11b). It increases in intensity and transforms into a resolved band at 640−670 cm^{-1} after 2.5 h of DP (Figure 11c), which becomes narrower and centered at 670 cm^{-1} beyond 4 h of DP (Figure 11f).

4. Two strong bands at 1050 and 1000 cm^{-1} are clearly visible beyond 16 h of DP (Figure 11f); they are characteristic of ν_{Si-O} vibration of an ill-crystallized 1:1 nickel phyllosilicate (Figure 6c). The band at 3645 cm^{-1} whose resolution has improved meanwhile (Figure 11f), may be attributed to the ν_{OH} vibration of 1:1 nickel phyllosilicate whose crystallinity increases with time; the possible formation of 2:1 nickel phyllosilicate can be ruled out because the $I_{670\ cm^{-1}}/I_{1000\ cm^{-1}}$ ratio in Ni/XOA400 (50 h), equal to 0.58, is closer to that of a 1:1 nickel phyllosilicate than of a 2:1 nickel phyllosilicate (Table 4).

5. The band of δ_{H_2O} at 1630 cm^{-1} increases.

6. The small band at 1385 cm^{-1}, due to the presence of small amount of nitrates, does not change significantly beyond 4 h of DP.

7. The narrow band at 2205 cm^{-1}, which shifts down to 2185 cm^{-1} while its intensity increases, is due to the presence of NCO^- isocyanate anions. This point will be developed later on.

These observations lead to the following remarks:

1. For a DP time <4 h, the DP Ni(II) phase in Ni/XOA400 samples is probably a mixture of nickel hydroxide and 1:1 nickel phyllosilicate. The formation of 1:1 nickel phyllosilicate is attested by the fact that the IR band in the δ_{OH} vibration range (Figure 11c) exhibits a shoulder at 670 cm^{-1} (Figure 6), while that of nickel hydroxide is attested by a shoulder at 640 cm^{-1} (Figure 4). Beyond 4 h of DP, the band at 670 cm^{-1} is associated to two bands at 1050 and 1000 cm^{-1}, characteristic of a 1:1 nickel phyllosilicate (Figure 6c,d); 2:1 nickel phyllosilicate should have provided a single vibration at 1020 cm^{-1} (Figure 6a,b).

2. The surface silanol groups are involved into the mechanism of interaction between Ni(II) and silica, as attested by the decrease and disappearance of the asymmetric ν_{Si-OH} band at 980 cm^{-1} after 2.5 h of DP (Figure 11c).

3. The formation of 1:1 nickel phyllosilicates leads to deep changes in the silicic network and finally to its destruction, as indicated by the disappearance of the bands at 1100 and 800 cm^{-1} after 16 h of DP (Figure 11f). Hence, the silica support is gradually eroded during deposition−precipitation and finally completely consumed. Silica consumption and nickel silicate formation have also been reported by Geus[53] and observed by IR on samples prepared by precipitation involving the addition of nickel sulfate and sodium carbonate in a vessel containing silica slurry.[54−56]

The hypothesis of the precipitation of a basic nickel carbonate as in the case of the precipitation in the absence of silica may be excluded. Indeed, the IR bands of carbonates between 830 and 1610 cm^{-1} are not visible in Figure 11, in contrast with Figure 4. In addition, it may be noted that when a suspension of basic nickel carbonate and silica in distilled water is maintained at 90 °C during 24 h, bulk 1:1 nickel phyllosilicate is formed.

The IR spectra obtained with the Ni/XO30LS samples after different times of deposition-precipitation are given in Figure 12. The silica vibration bands evolve in the same way as those in Ni/XOA400 samples (Figure 11): (i) decrease of the bands of silicic network (1000 and 800 cm^{-1}); (ii) appearance of the bands at 1050 and 1005 cm^{-1}, characteristic of the ν_{SiO} bands of ill-crystallized 1:1 nickel phyllosilicate.

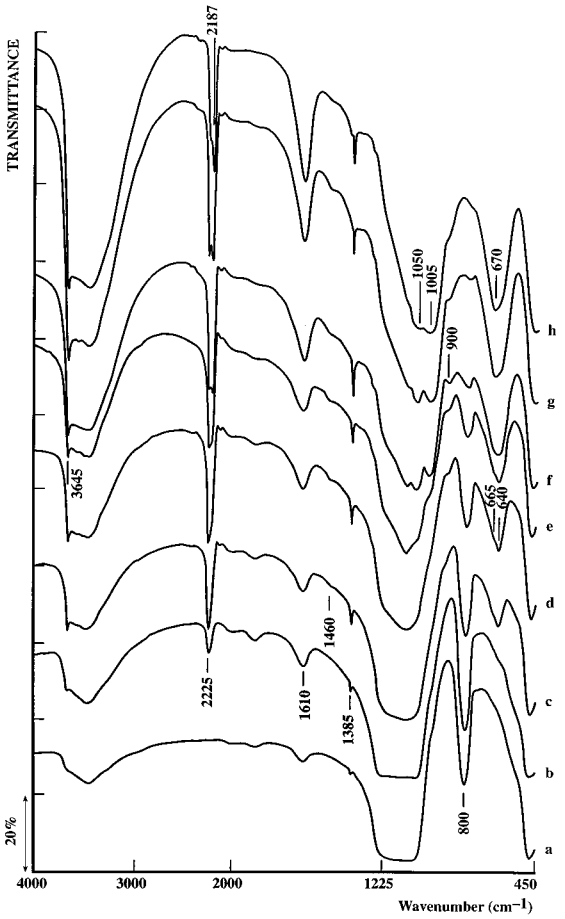

Figure 12. IR spectra of of Ni/XO30LS after different times of deposition−precipitation: (a) $t = 0$; (b) 70 min; (c) 2.5 h; (d) 4 h; (e) 8 h; (f) 16 h; (g) 24 h; (h) 50 h.

However, some differences may be observed in the frequency range of δ_{OH}: for 2.5 and 4 h of DP, a narrow band at 640 cm^{-1} is visible with a shoulder at ≈665 cm^{-1} (Figure 12c,d), indicating that the DP Ni(II) phase is a mixture of nickel hydroxide (640 cm^{-1}) and of nickel phyllosilicate (670 cm^{-1}). It may be reminded that quantitative contribution of the different Ni(II) phases is not straightforward from the IR spectra. This interpretation also suggests that the ν_{OH} vibration band at 3645 cm^{-1}, visible at short DP time (≤4 h), arises from surface hydroxyls of nickel hydroxide and 1:1 nickel phyllosilicate. However, when the band at 670 cm^{-1} becomes clearly visible beyond 16 h of DP, and associated with the bands at 1005 and 1050 cm^{-1} (Figure 12f−h), the band at 3645 cm^{-1} may be assigned to the ν_{OH} of a 1:1 nickel phyllosilicate as in the case of the Ni/XOA400 samples. It may be noted that this band is better resolved than in Ni/XOA400 samples, indicating a higher crystallinity of the 1:1 nickel phyllosilicate on silica XO30LS.

Another difference between the Ni/XOA400 and Ni/XO30LS samples is the different intensities of the bands corresponding to the anionic species.

The vibration band of isocyanates at about 2200 cm^{-1} increases more strongly in Ni/XO30LS versus the DP time (Figure 12) than in Ni/XOA400 (Figure 11). However, it may be noted that the shape and frequency of the isocyanate band change versus DP time for the Ni/XO30LS samples:

(i) below 8 h of DP, the band is asymmetric with a maximum at 2225 cm^{-1} (Figure 12b−d);

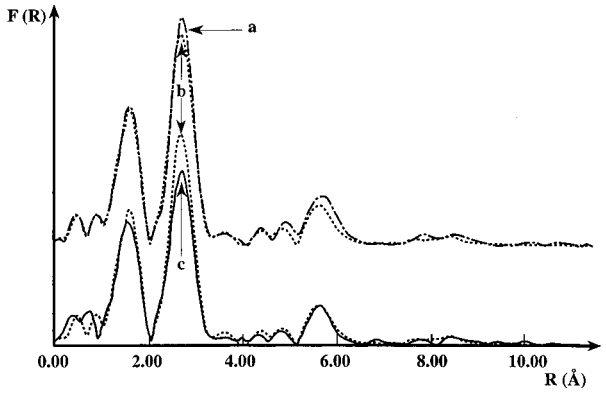

Figure 13. Fourier transform (k^3-weighted, without phase correction) of the experimental EXAFS signals of (a) Ni/XOA400 (70 min) (− · − · −); (b) Ni/XOA400 (4 h) (···); (c) Ni/XO30LS (4 h) (—)

(ii) after 8 h, the band splits into two bands at 2225 and 2205 cm^{-1} (Figure 12e);

(iii) beyond 16 h, the band at 2225 cm^{-1} decreases while that at 2205 cm^{-1} shifts toward smaller wavenumbers (Figure 12g,h); beyond 50 h of DP (Figure 12h), the second band is the strongest one and is shifted to 2187 cm^{-1}; its frequency is the same as that in Ni/XOA400 (50 h) (Figure 11h), i.e., when the Ni(II) phase is a bulk 1:1 nickel phyllosilicate.

In consequence, it may be proposed that the band at 2225 cm^{-1} is due to isocyanate ions located in the α-$Ni(OH)_2$ structure while the band, shifting between 2205 and 2187 cm^{-1}, corresponds to isocyanates located in 1:1 nickel phyllosilicates; the shift should be due to a change in the isocyanate environment because of the increasing crystallinity of the nickel phyllosilicate.

As for the isocyanate band, the nitrate vibration band at 1385 cm^{-1} increases more strongly in Ni/XO30LS (Figure 12) than in Ni/XOA400 (Figure 11).

The intensity of the anionic vibration bands larger, in Ni/XO30LS (Figure 12) than in Ni/XOA400 (Figure 11), is consistent with the formation of an hydroxide phase with anionic species in the interlayer spacing for short DP time. It may be noted that the nickel hydroxide formula is slightly different from that obtained in the absence of silica because of the higher proportion of isocyanates and the lower one of nitrates and the absence of carbonates.

The nitrate and isocyanate vibration bands do not disappear after long time of DP on either silica XOA400 or XO30LS, i.e., when the 1:1 nickel phyllosilicate is formed. Since the layers of 1:1 nickel phyllosilicate are known to be neutral with no ion exchange capacity, the presence of anionic species between the layers cannot be evoked. However, Decarreau et al.[45,50] have noted that during hydrothermal synthesis of nickel phyllosilicates at low temperature (low-crystallinity), some chlorine or nitrate anions arising from the $NiCl_2$ or $Ni(NO_3)_2$ precursors, respectively, are present in the final compound and cannot be eliminated, even by thorough washing. According to these authors, the anionic species could be trapped in the structure of the 1:1 nickel phyllosilicate during preparation.

c. EXAFS Technique. Two Ni/XOA400 (70 min, 5.2 wt % Ni and 4 h, 25.1 wt % Ni) and one Ni/XO30LS samples (4 h, 21.3 wt % Ni) have been studied by EXAFS. The Fourier transforms of the EXAFS signals are shown in Figure 13 while those of the reference samples, i.e., the 1:1 and 2:1 nickel phyllosilicates synthesized at 150 °C, are shown in Figure 14. The Fourier backtransforms of the second neighbor peak are reported in Figures 15 and 16. The EXAFS signal treatments, the simulation of the second peak of the Fourier transforms and of their backtransforms led to the results gathered in Table 5. It

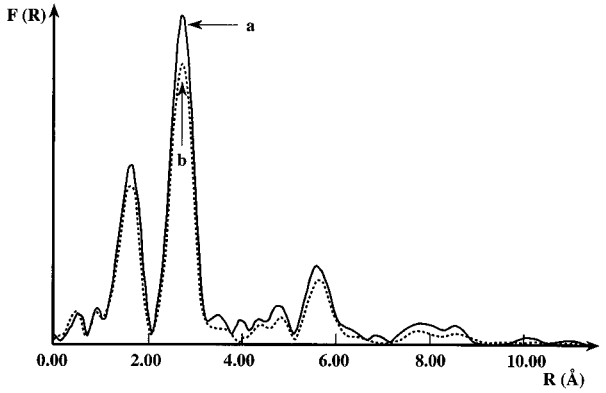

Figure 14. Fourier transform (k^3-weighted, without phase correction) of the experimental EXAFS signals of (a) 2:1 nickel phyllosilicate synthesized at 150 °C (—); (b) 1:1 nickel phyllosilicate synthesized at 150 °C (···).

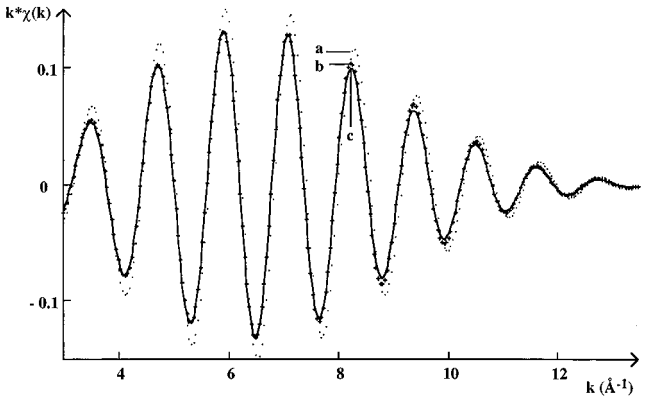

Figure 15. Fourier backtransforms of the second neighbor peak of (a) 1:1 nickel phyllosilicate synthesized at 150 °C (···); (b) Ni/XOA400 (70 min) (+++); (c) Ni/XOA400 (4 h) (—).

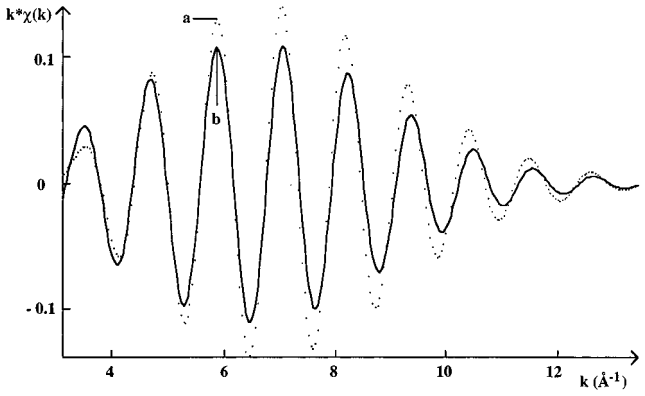

Figure 16. Fourier backtransforms of the second neighbor peak of (a) β-$Ni(OH)_2$ (···); (b) Ni/XO30LS (4 h) (—).

may be noted that the number of second neighbors in the reference samples is found smaller than that expected, i.e., 6 Ni and 2 Si for 1:1 nickel phyllosilicate and 6 Ni and 4 Si for 2:1 nickel phyllosilicate. This difference was widely discussed by Carriat[51] in an EXAFS study on 1:1 and 2:1 nickel phyllosilicates synthesized at various temperatures (25−500 °C). According to Carriat, the smaller number of backscatterers obtained with poorly crystallized nickel phyllosilicates (25−150 °C) is due to the small domains of coherency in these compounds.

The Fourier transforms of the EXAFS signals of Ni/XOA400 (70 min) and Ni/XOA400 (4 h) (Figure 13a,b) are almost superimposable, which indicates that the same Ni(II) phase is present in these samples. The results given in Table 5 show

TABLE 5: Fitted Structural Parameters of 2:1 and 1:1 Nickel Phyllosilicates Synthesized at 150 °C, Ni/XOA400 (70 min), Ni/XOA400 (4 h), and Ni/XO30LS (4 h), Determined by EXAFS at the Ni K Edge for the Second Shell

compounds	neighbors	N	R (Å)	γ (Å^{-2})[a]	σ (Å)	fit
2:1 nickel phyllosilicate (150 °C)	Ni	5.8	3.06	1.00	0.068	1.8×10^{-3}
	Si	3.7	3.26	0.85	0.095	
1:1 nickel phyllosilicate (150 °C)	Ni	5.6	3.08	1.00	0.071	2.0×10^{-3}
	Si	2.0	3.30	0.85	0.093	
Ni/XOA 400 (70 min, 5.2 wt % Ni)	Ni	5.3	3.10	1.00	0.072	1.1×10^{-3}
	Si	2.0	3.30	0.85	0.114	
Ni/XOA 400 (4 h, 25.1 wt % Ni)	Ni	5.4	3.10	1.00	0.075	1.8×10^{-3}
	Si	2.0	3.30	0.85	0.115	
Ni/XO30LS (4 h, 21.3 wt % Ni)	Ni	5.1	3.10	1.00	0.078	2.4×10^{-3}

[a] Fixed parameters.

that the Ni(II) phase may be attributed to a 1:1 nickel phyllosilicate, and not to a 2:1 nickel phyllosilicate or a nickel hydroxide. This is emphasized by the fact that the Fourier backtransforms of the second neighbor peak (Figure 15b,c) fit well with that of a 1:1 nickel phyllosilicate synthesized at 150 °C (Figure 15a). These EXAFS results are also in agreement with those obtained by Clause et al.[5] on deposited−precipitated Ni/XOA400 samples after different DP times (1 h, 2.5 wt % Ni; 3 h, 7.5 wt % Ni; 72 h, 17.5 wt % Ni).

The comparison of the Fourier transforms of the EXAFS signals of Ni/XOA400 (4 h) and Ni/XO30LS (4 h) shows that the second peak of Ni/XO30LS (4 h) is relatively less intense than that of Ni/XOA400 (4 h) (Figure 13b,c), suggesting that the number of second neighbors is smaller. The simulation of the second peak of Ni/XO30LS (4 h) was impossible as long as a small number of Si (<0.1) was introduced. The best fit was obtained without Si contribution. Therefore, it may be deduced that the Ni(II) phase in Ni/XO30LS (4 h) is mainly an hydroxide; the number of Ni neighbors is found to be smaller than 6, probably because of the nonstoichiometry of the $Ni(OH)_{2-x}$ layers and the low-crystallinity of the turbostratic nickel hydroxide. However, the Fourier backtransform of the second neighbor peak (Figure 16) does not fit well with that of the β-$Ni(OH)_2$ reference. The contribution of the second neighbors at $k \leq 4$ is higher in Ni/XO30LS (4 h) than in nickel hydroxide, indicating the possible presence of a small amount of nickel phyllosilicates. Indeed, the contribution of Si neighbor is relatively higher than that of Ni at $k \leq 4$. The presence of phyllosilicates would also explain that the fit value is not as good as that of the Ni/XOA400 samples.

d. Temperature-Programmed Reduction. The TPR profiles of the Ni/XO30LS samples obtained for DP times shorter than 4 h (Figure 17a−c) exhibit one asymmetric peak at 380 °C with a shoulder at 400−450 °C. Beyond 4 h of DP (Figures 17d-f), the 380 °C peak intensity decreases while the shoulder transforms into a broad peak, which increases in intensity and shifts toward higher temperature (up to ≈670 °C).

The TPR profiles of the Ni/XOA400 samples obtained for DP times shorter than 100 min (Figure 18a,b) exhibit a broad peak at about 460 °C with a shoulder at about 380 °C. For 2.5 and 4 h of DP (Figure 18c,d), the shoulder disappears while the broad peak increases and shifts toward higher temperatures. Similar TPR profiles have been obtained in the literature[5,22,24,26,31] on analogous samples. Then, for very long DP time (50 and 100 h), the broad peak splits into two bands at 560 and 620 °C (Figure 18e,f).

The broad TPR peak of Ni/XOA400, which shifts to higher temperature and splits when DP time increases (Figure 18), may be attributed to 1:1 nickel phyllosilicate according to the reference samples (Figure 7) and the results described above. It may be noted that it is well-known that supported nickel phyllosilicates are reducible at higher temperature than unsupported ones and that supported 2:1 nickel phyllosilicate is less reducible than supported 1:1 nickel phyllosilicate; it exhibits a broad peak with a maximum between 600 and 800 °C.[10,51] The temperature difference is due to the interaction with the support, which lowers the Ni(II) reducibility, as often observed for supported oxides. The TPR peak shift to higher temperature

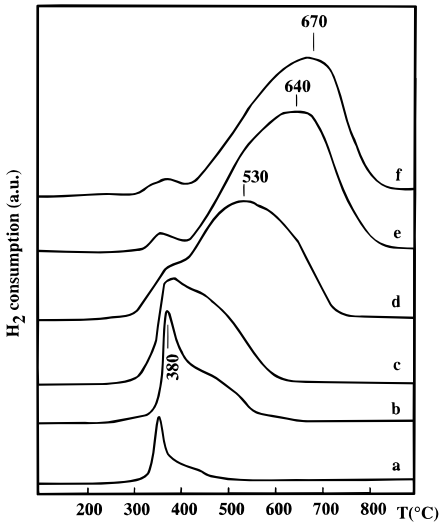

Figure 17. TPR profiles of Ni/XO30LS samples after different times of deposition−precipitation: (a) 70 min; (b) 2.5 h; (c) 4 h; (d) 16 h; (e) 50 h; (f) 100 h.

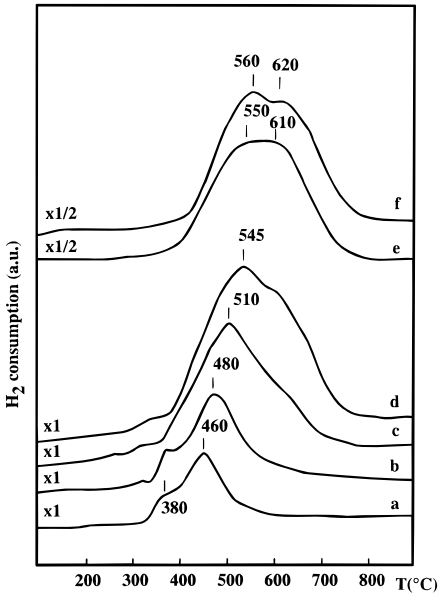

Figure 18. TPR profiles of Ni/XOA400 samples after different times of deposition−precipitation: (a) 70 min; (b) 100 min; (c) 2.5 h; (d) 4 h; (e) 50 h; (f) 100 h.

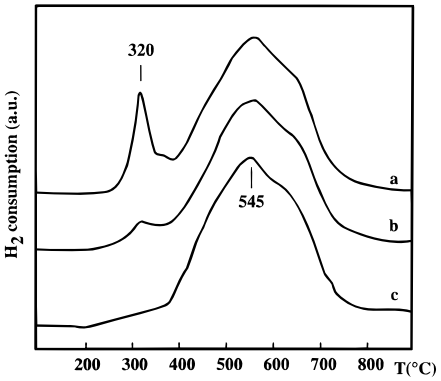

Figure 19. TPR profiles of Ni/XOA400 (4 h): (a) unwashed after filtration of the reaction mixture at 90 °C; (b) unwashed after filtration of the reaction mixture cooled to 25 °C; (c) washed after filtration of the reaction mixture cooled to 25 °C.

versus the DP time is due to the increasing crystallinity of the phyllosilicate, as attested by the XRD and IR results.

The shoulder at 400−450 °C observed on Ni/XO30LS at short DP times (Figure 17a−c), which becomes a broad peak beyond 4 h of DP (Figure 17d,e) and shifts toward higher temperature with DP time, may be also attributed to the reduction of 1:1 nickel phyllosilicate.

According to the results obtained by XRD, IR, and EXAFS, the DP Ni(II) phase in Ni/XO30LS is mainly a nickel hydroxide with turbostratic structure for DP times shorter than 4 h. Therefore, the peak at 380 °C may be attributed to the reduction of this supported phase. This peak is also present as a shoulder in the TPR profiles of Ni/XOA400 (70 and 100 min) (Figure 18a,b), which indicates that nickel hydroxide is also formed on silica XOA400 for very short DP times. As already noticed for supported and unsupported phyllosilicates, nickel hydroxide (Figure 7a) is reduced at lower temperature (320 °C) than in the presence of silica (380 °C).

As mentioned in the experimental section, cooling the mixture from 90 to 25 °C is crucial to solubilize nickel bicarbonate precipitated on silica during deposition−precipitation at 90 °C. This is exemplified by the presence of a TPR peak at 320 °C in the unwashed Ni/XOA400 (4 h) sample collected after filtration of the uncooled mixture (Figure 19a). The peak is almost gone when the unwashed sample is cooled to 25 °C before filtration (Figure 19b). The washing step after filtration of the cooled solution permits the complete elimination of this peak (Figure 19c). This peak is tentatively attributed to the reduction of a precipitate of nickel bicarbonate formed from the reaction between Ni^{2+} complexes in solution and HCO_3^- arising from urea hydrolysis (eq I). This interpretation is emphasized by the work of Smurov[57] who mentioned that solubility of $Ni(HCO_3)_2$ in water containing CO_2 increases drastically when the temperature decreases (80 to 5 °C).

e. Electron Microscopy: TEM and STEM-EDX. The electron micrographs of Ni/XOA400 (≤4 h) samples exhibit filandrous structure with a high number of small and thin platelets dispersed on the silica surface with random orientations, as exemplified in the case of Ni/XOA400 (4 h) (Figure 20a). Most of them consist of stacks of 2−5 layers of 150−250 Å long and ≈20−40 Å thick, with a lattice spacing of ≈9 Å, which may be consistent with the presence of 1:1 nickel phyllosilicate. The platelet thickness does not seem to increase drastically with the nickel loading for short DP time (≤4 h). This filandrous structure has been already observed on similar samples.[5,15,16,23,24,29]

In the case of Ni/XO30LS, two types of structures are observed for short DP time (≤4 h) (Figure 20b): (i) thin platelets of 2−4 layers (≈20−30 Å thick), or more sometimes, which follow the shape of the silica particles; the platelets are rather difficult to observe; (ii) large and thicker platelets (500−1000 Å long and 40−100 Å thick) fixed on the silica surface but protruding outward from it. The former structure is most often observed but some silica particles or part of them seem to be uncovered. The lattice spacing is about 8 Å, which may be consistent with the presence of nickel hydroxide. It may be noted that the stacks are easily decomposed under electron beam, in contrast with those of Ni/XOA400 samples, confirming that the layered compound in Ni/XO30LS is different in nature from that in Ni/XOA400.

STEM-EDX analyses were performed on Ni/XOA400 (4 h) and Ni/XO30LS (4 h). The Ni and Si atomic percentages have been measured over about 15 spots with an analyzer of 150 Å diameter. Ni and Si distributions on Ni/XOA400 (4 h) are rather homogeneous (Table 6), indicating that silica is rather uniformly covered by nickel phyllosilicates. In contrast, Ni and Si distributions are much less homogeneous on Ni/XO30LS (4 h). It may be noted that the analysis of uncovered parts of silica XO30LS reveals the presence of nonnegligible amounts of Ni, which could be present as a layer of brucitic Ni in epitaxy with silica, as already suggested by Coenen.[22]

Beyond 50 h of DP, electron micrographs of Ni/XOA400 (100 h) (Figure 20c) and Ni/XO30LS (100 h) (Figure 20d) appear more similar. They no longer exhibit any more silica particles but a dense filandrous structure of layered compounds with platelets with 5−20 layers. Ni/XO30LS (100 h) and Ni/XOA400 (100 h) differ in that some platelets look thinner and longer in the former sample. The lattice spacing of the platelets is about 8 Å for each sample, which is consistent with the XRD results.

f. BET Surface Area Measurements. Figure 8 reports the changes in the surface areas of Ni/XOA400 and Ni/XO30LS samples versus the DP time as well as those of silicas XOA400 and XO30LS submitted to the same DP treatment, but without nickel nitrate.

First, it may be noted that for both silicas and whatever the DP time, the surface area of Ni/SiO_2 is higher than that of the silica alone. This has been also observed by several authors[16,24,25,29] in the case of deposited−precipitated Ni(II) on silica of high surface area. These results indicate that the layered structure of the DP Ni(II) phase develops a new surface area.

Considering silica alone, it may be observed that the surface area of silica XOA400 decreases versus the time of urea decomposition at 90 °C (Figure 8b). According to Hénin and Robichet[58] and Iler,[59] a basic solution induces the dissolution of silica and an increase in silica particle size because of (i) the dissolution of the smallest silica particles to the benefit of the largest ones (Ostwald ripening) and (ii) the aggregation or coalescence of particles. Hence, the decrease in the XOA400 surface area may be due to a loss of porosity and an increase in the particle size. The constancy of the XO30LS surface area (Figure 8d) is probably related to the fact that the surface area was initially too low (larger pores, larger particles) to be significantly affected by the basification of the solution.

Considering now the Ni/SiO_2 samples, it may be observed that the surface area of Ni/XOA400 increases up to about 4 h of DP and then decreases (Figure 8a). This result may be explained as follows: (i) for short DP times (<4 h), the DP Ni(II) phase, which consists of thin platelets of 1:1 nickel phyllosilicates with random orientations, induces an increase in the surface area (Figure 20a); (ii) beyond 4 h, the increasing amount of nickel phyllosilicate induces a deep alteration of the silicic network, which contributes to a decrease in the overall

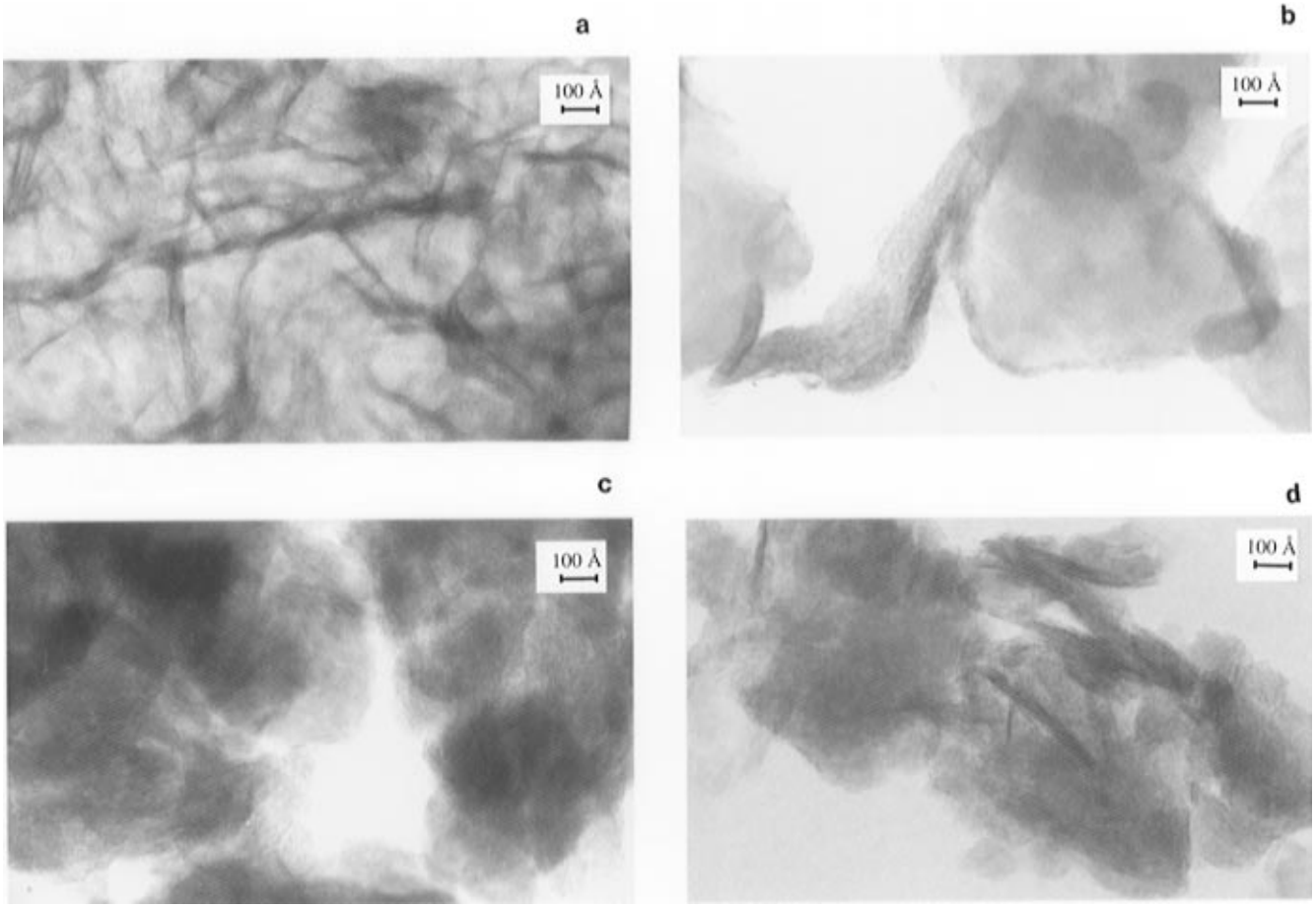

Figure 20. TEM micrographs of (a) Ni/XOA400 (4 h); (b) Ni/XO30LS (4 h); (c) Ni/XOA400 (100 h); (b) Ni/XO30LS (100 h).

TABLE 6: STEM-EDX Results Obtained with Ni/XOA 400 (4 h) and Ni/XO30LS 4h

samples	atom %	Ni	Si	remarks
Ni/XOA 400 (4 h)	extreme values	26	74	
		34	66	
	average value	29	71	
Ni/XO30LS (4 h)	extreme values	76	24	← focalization on a platelet
		11	90	← uncovered silica
	average value	35	65	

surface area (Figure 20c). Meanwhile, the crystallinity of the DP Ni(II) phase increases, as attested by the XRD, IR, and TPR results, and the platelets become thicker (Figure 20c); these changes probably also contribute to the lowering of the sample surface area.

In the case of the Ni/XO30LS samples (Figure 8c), the BET surface area always increases with the DP time. The increase may be related to the increasing amount of layered compounds formed, first of α-$Ni(OH)_2$ up to 4 h of DP, then of 1:1 nickel phyllosilicate, which both develop new surface area because of their disordered stacking.

4. Characterization of the Nickel(II) Phase Deposited−Precipitated on Nonporous Silicas and Comparison with Porous Silica. Two Ni/SiO_2 (2.5 h) samples have been prepared with nonporous silicas AD380 (380 $m^2 \cdot g^{-1}$) and OX50 (50 $m^2 \cdot g^{-1}$), which exhibit almost the same surface areas as the porous ones. Their Ni loadings, 17.2 and 14.7 wt % Ni, respectively, are very close to those obtained on porous silicas (Table 1).

The IR spectra of Ni/AD380 (2.5 h) (Figure 21a) and Ni/OX50 (2.5 h) (Figure 21b) are also very similar to those of Ni/XOA400 (2.5 h) (Figure 11c) and Ni/XO30LS (2.5 h) (Figure 12c), respectively. However, the shoulder at 670 cm^{-1} in Ni/OX50 (2.5 h) (Figure 21b) seems to be more intense than in Ni/XO30LS (2.5 h) (Figure 12c) and rather similar to that in Ni/XO30LS (18 h) (Figure 12e).

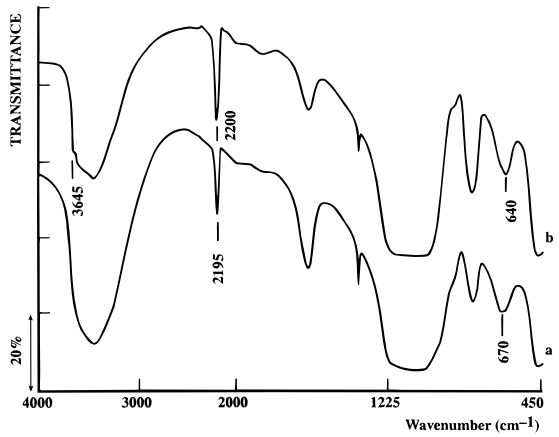

Figure 21. IR spectra of (a) Ni/AD380 (2.5 h) and (b) Ni/OX50 (2.5 h).

The XRD pattern of Ni/AD380 (2.5 h) (Figure 22a) exhibits a 001 line as a shoulder at 11.5 Å, which was not observed on Ni/XOA400 (2.5 h) (Figure 9b). The basal spacing is as large as that of the ill-crystallized 1:1 nickel phyllosilicate synthesized at 25 °C (Figure 5b). The XRD pattern of Ni/OX50 (2.5 h) (Figure 22b) exhibits a broad 001 line at 8.93 Å; this line was thinner, smaller and at 7.25 Å in Ni/XO30LS (2.5 h) (Figure 10b).

The TPR peaks of Ni/AD380 (2.5 h) and Ni/OX50 (2.5 h) samples (Figure 23) exhibit maxima at higher temperature than those of Ni/XOA400 (2.5 h) (Figure 18c) and Ni/XO30LS (2.5 h) (Figure 17b), respectively: 410 °C for Ni/OX50 (2.5 h)

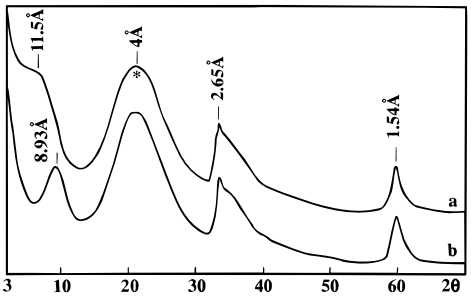

Figure 22. XRD patterns of (a) Ni/AD380 (2.5 h) and (b) Ni/OX50 (2.5 h) (*, silica).

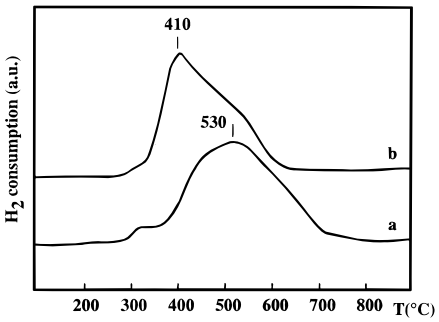

Figure 23. TPR profiles of (a) Ni/AD380 (2.5 h) and (b) Ni/OX50 (2.5 h).

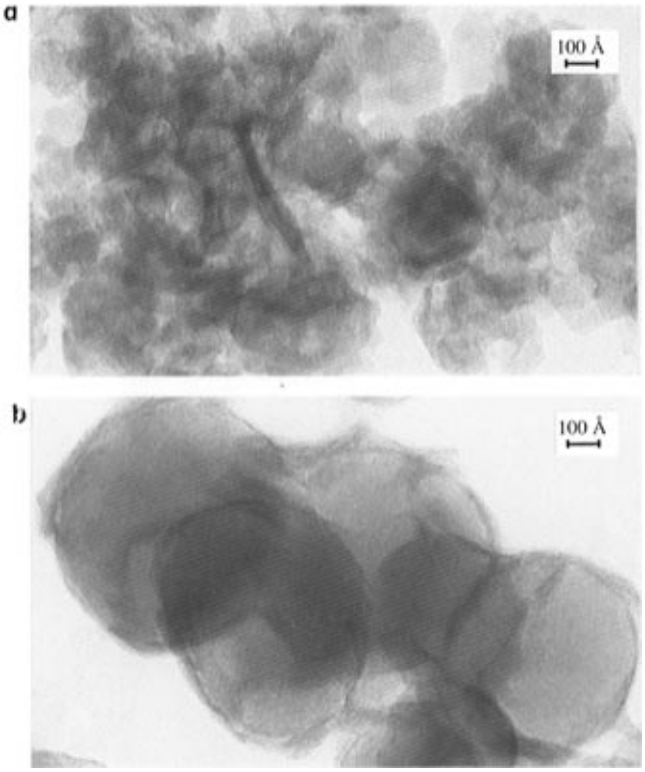

Figure 24. TEM micrographs of (a) Ni/AD380 (2.5 h); (b) Ni/OX50 (2.5 h).

instead of 380 °C for Ni/XO30LS (2.5 h), and 530 °C for Ni/AD380 (2.5 h) instead of 480 °C for Ni/XOA400 (2.5 h). In addition, the shoulder at about 500 °C in the TPR profile of Ni/OX50 (2.5 h) (Figure 23b) is relatively more intense than that in Ni/XO30LS (2.5 h) (Figure 17b).

The TEM micrographs of Ni/AD380 (2.5 h) sample (Figure 24a) exhibit platelets thicker (3−10 layers, 40−80 Å thick, lattice spacing ≈8 Å) than in Ni/XOA400 (Figure 20a). Some of them are flat, like those on Ni/XOA400, but others are curved and seem to follow the shape of the silica particles. The structure does not appear as filandrous as is the case of Ni/XOA400 (Figure 20a). The DP Ni(II) phase in Ni/OX50 (2.5 h) consists of platelets of several layers (≈8 Å of lattice spacing), which all follow the shape of the silica particles (Figure 24b) in contrast with Ni/XO30LS (Figure 20b). Hence, the Ni(II) phase seems to be in closer interaction with the support than with silica XO30LS. In addition, they are also more visible than on Ni/XO30LS.

With silica of high surface area and after 2.5 h of DP, the same DP Ni(II) phase is formed on nonporous silica (AD380) as on porous one (XOA400), i.e., mainly a 1:1 nickel phyllosilicate. Indeed, the same IR spectrum was obtained with a band at 670 cm^{-1} (Figures 11c and 21a). However, the DP Ni(II) phase is better crystallized on nonporous silica than on porous one: (i) the XRD pattern of Ni/AD380 (2.5 h) exhibits a 001 line, which is not observed with Ni/XOA400 (2.5 h); that indicates that the 1:1 nickel phyllosilicate is better organized along the *c* axis on silica AD380 than on silica XOA400; (ii) TEM micrographs do not exhibit filandrous structures, in contrast with Ni/XOA400; (iii) the TPR peaks are shifted toward higher temperature. It may be suggested that because of the more regular geometry of the particles of silica AD380 than those of XOA400, the interface between silica and the Ni(II) phase is larger. Hence, the growth of more organized nickel phyllosilicates with a more regular stacking of the layers, i.e., with a higher crystallinity, is favored.

In contrast, the nature of the DP Ni(II) phase is somewhat different between nonporous and porous silicas with low surface area: the 1:1 nickel phyllosilicate/nickel hydroxide ratio is larger in Ni/OX50 (2.5 h) than in Ni/XO30LS (2.5 h): (i) the intensity ratio of the IR bands $I_{670\ cm^{-1}}/I_{640\ cm^{-1}}$ is higher; (ii) the XRD 001 line at 8.93 Å and its broadness, better correspond to 1:1 nickel phyllosilicate than to nickel hydroxide; (iii) the shoulder at 450−500 °C of the TPR profile is more intense. As in the case of silica of high surface area, the Ni(II) phase is better crystallized on nonporous than on porous silica: no platelets are protruding outward from the silica surface; the TPR peaks of both nickel hydroxide and 1:1 nickel phyllosilicate are shifted toward higher temperature. The reducibility of the Ni(II) phase lower in Ni/OX50 than in Ni/XO30LS, may be also due to the larger interface with silica, arising from the more regular shape of the silica particles.

5. Characterization of the Nickel(II) Phase Deposited−Precipitated on Silicas and Subjected to Hydrothermal Treatments. Up to now, the 1:1 nickel phyllosilicate is the only type of phyllosilicate formed during deposition−precipitation. Experiments to obtain 2:1 nickel phyllosilicate have been performed by changing the starting concentration of silica, and nickel nitrate or urea,[33] and by modifying the conditions of deposition−precipitation (injection of silicate solution, ultrasonic precipitation, delayed or slow addition of nickel nitrate solution, strong acidification of the starting solution[60]). The formation of 2:1 nickel phyllosilicate was never observed. It appears that only a hydrothermal treatment can lead to the transformation of 1:1 nickel phyllosilicate into 2:1 nickel phyllosilicate.

The Ni/XOA400 (4 h) sample was immersed in distilled water (3 $g{\cdot}L^{-1}$), and the suspension was introduced in a Teflon autoclave. The hydrothermal treatment, conducted at 120 or 190 °C during 7 days, induces the formation of a less reducible Ni(II) phase than just after deposition-precipitation (Figure 25). Indeed, Ni/XOA400 (4 h) provides a TPR peak at 565 °C (Figure 25a) while after hydrothermal treatment at 190 °C, the TPR profile exhibits an asymmetric reduction peak with a maximum at 755 °C (Figure 25c), characteristic of the reduction of a well-crystallized 2:1 nickel phyllosilicate obtained by hydrothermal synthesis at 200 °C.[44,51] The TPR profile of the

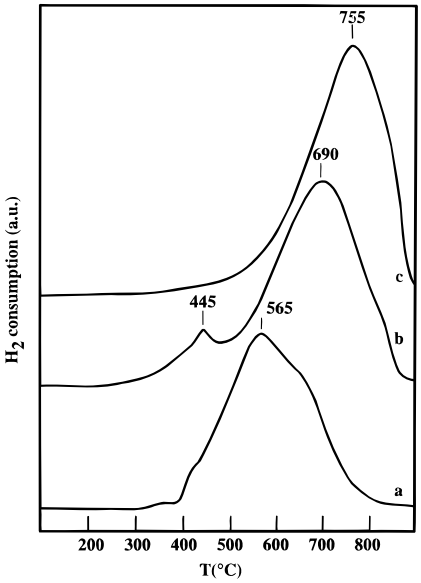

Figure 25. TPR profiles of (a) Ni/XOA400 (4 h); (b) (a) then hydrothermal treatment at 120 °C during 7 days; (c) (a) then hydrothermal treatment at 190 °C during 7 days.

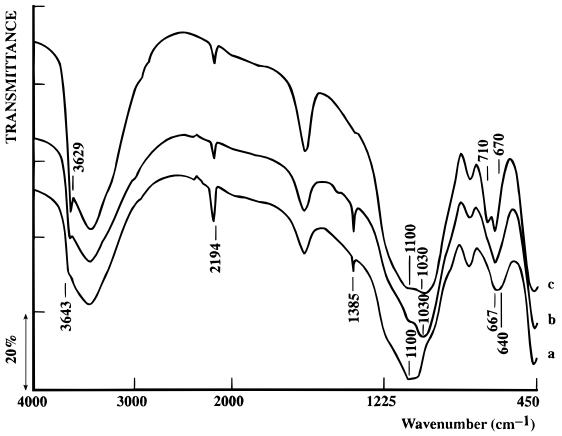

Figure 26. IR spectra: (a) Ni/XOA400 (4 h); (b) (a) after hydrothermal treatment at 120 °C during 7 days; (c) (a) after hydrothermal treatment at 190 °C during 7 days.

sample treated at 120 °C exhibits a broad peak at 690 °C and a smaller one at 445 °C (Figure 25b), corresponding to a mixture of 2:1 and 1:1 nickel phyllosilicates, respectively, with a higher proportion of the former. This 2:1 nickel phyllosilicate is less crystallized than after hydrothermal treatment at 190 °C, as indicated by the lower reduction temperature peak.

These changes have been confirmed by IR spectroscopy (Figure 26), i.e., the gradual appearance of the vibration bands characteristic of 2:1 nickel phyllosilicate at about 3625, 1030, 710, and 670 cm^{-1} (see section 2b and Figure 6b). In addition, the nitrate vibration band at 1385 cm^{-1} disappears while that of isocyanates at about 2200 cm^{-1} decreases significantly. It may be noted that the broad band at about 1000 cm^{-1} remained because of the presence of unreacted silica.

Discussion

The nature of the DP Ni(II) phase depends on both the silica surface area and the DP time (Table 7). For long DP time (>4 h), the DP Ni(II) phase is a 1:1 nickel phyllosilicate, whether the silica surface area is low (≈50 $m^2 \cdot g^{-1}$) or high (≈400 $m^2 \cdot g^{-1}$). It contains nitrate and isocyanate anions entrapped in the structure. The crystallinity of the nickel phyllosilicates is low, as attested by the presence in the IR spectra of a shoulder at 900−910 cm^{-1} (Figures 11 and 12) which is also observed in the spectrum of 1:1 nickel phyllosilicate synthesized at 25 °C (Figure 6c), and commented on in section 2b. The low crystallinity is also attested by the XRD patterns (Figures 9 and 10). This result is not surprising since even after a hydrothermal synthesis at 200 °C, bulk nickel phyllosilicate is not yet very well-crystallized.[45] However, 1:1 nickel phyllosilicate is better crystallized when it arises from silica of low surface area than from silica of high surface area, as indicated by the better resolved XRD lines (Figures 9d,e and 10d,e), the better resolved ν_{OH} vibration band at 3645 cm^{-1} (Figures 11e−h and 12e−h), and the higher reduction temperature (Figures 17e,f and 18e,f). In addition, the silica surface area has an influence on the morphology of the nickel phyllosilicates formed (Figures 20c,d) since they lead to different BET surface area after deposition-precipitation (Figure 8).

For short DP time (≤4 h), the nature of the DP Ni(II) phase depends on the silica surface area. As indicated by the different techniques and especially by the EXAFS, the Ni(II) phase supported on silica of high surface area is a 1:1 nickel phyllosilicate with a small proportion of nickel hydroxide at very short DP time (≤100 min). In contrast, the Ni(II) phase supported on silica of low surface area (≤4 h) is mainly a nickel hydroxide with a turbostratic structure and contains a small amount of 1:1 nickel phyllosilicate. When deposition−precipitation proceeds and Ni loading increases, the proportion of 1:1 nickel phyllosilicate increases, as if nickel hydroxide was gradually transformed into 1:1 nickel phyllosilicate. Supported turbostratic nickel hydroxide is slightly different from that obtained in the absence of silica since it does not contain intercalated carbonate ions, but only nitrate and isocyanate anions. It may be noted that the lattice spacings between the platelets, measured by TEM, are consistent with those deduced from the 001 reflections of the XRD patterns in Figures 9 and 10.

The formation of a 1:1 nickel phyllosilicate has also been observed in earlier works in samples prepared by nickel deposition−precipitation on silica of high surface area,[5,15,16] while that of nickel hydroxide has been observed during nickel deposition-precipitation by urea hydrolysis on quartz plates (very low surface area).[61] However, the relevance of the silica surface area and of the DP time had never been rationalized before (Table 7).

From the results, it also appears that the porous or nonporous nature of silica has no influence on the Ni loading, and no strong influence on the nature of the DP Ni(II) phase, although the proportion of 1:1 nickel phyllosilicate is higher on nonporous than on porous silica of low surface area, for short DP time. It may be concluded that the porosity does not affect significantly the mechanism of deposition−precipitation. However, the silica porosity strongly influences the morphology, distribution, and crystallinity of the DP Ni(II) phase, independently of the silica surface area: most of the platelets of the Ni(II) phase supported on porous silica XOA400 exhibit random orientations or some of them protrude outward from the surface of porous silica XO30LS, while those supported on nonporous silicas (AD380 or OX50) better follow the shape of the silica particles and seem to exhibit a larger interface with the silica support. It may be noted that according to Coenen,[22] it is likely that at least a monolayer of nickel silicate serves at the interface of attachment between silica and hydroxide.

Sample characterization by XRD and IR has shown that independently of the surface area, silica is almost totally consumed beyond 16 h of DP (disappearance of the XRD broad band at about 4 Å, characteristic of amorphous silica (Figures

TABLE 7: Influence of the Silica Characteristics (Surface Area and Porosity) and the DP Time on the Nature of the Ni(II) Phase

surface area	silica porosity	origin	DP time	nature of the Ni(II) phase[a]	remarks
low (≈50 $m^2 \cdot g^{-1}$)	yes	XO30LS	≤4 h	supported nickel hydroxide	
			4−16 h	supported 1:1 nickel phyllosilicate	
			>16 h	bulk 1:1 nickel phyllosilicate	aging period: crystallinity increases with DP time
	no	OX50	2.5 h	mixture of supported 1:1 nickel phyllosilicate and supported nickel hydroxide	higher crystallinity than on XO30LS
high (≈400 $m^2 \cdot g^{-1}$)	yes	XOA400	≤100 min	supported 1:1 nickel phyllosilicate with small amount of supported nickel hydroxide	
			100 min−16 h	supported 1:1 nickel phyllosilicate	
			>16 h	bulk 1:1 nickel phyllosilicate	aging period: crystallinity increases with DP time; lower crystallinity than on XO30LS
	no	AD380	2.5 h	supported 1:1 nickel phyllosilicate	higher crystallinity than on XOA400

[a] 2:1 nickel phyllosilicate is only formed after hydrothermal treatment.

TABLE 8: Equilibrium Constant of 1:1 and 2:1 Nickel Phyllosilicates in Aqueous Solution, $Ni_3(OH)_4Si_2O_5 + 6\ H^+ \rightleftarrows 3\ Ni^{2+} + 2Si(OH)_4 + H_2O$ and $Ni_3(OH)_2(Si_2O_5)_2 + 6H^+ + 4H_2O \rightleftarrows 3Ni^{2+} + 4Si(OH)_4$, and Free Energy of Formation According to Refs 44, 62, and 63

		ΔG°_f	
	$-\log K_{298}$	kcal·mol^{-1}	kcal·g^{-1}
1:1 nickel phyllosilicate	16.8	≈−690	≈−1.8
2:1 nickel phyllosilicate	58.2	≈−1040	≈−2.5

9 and 10), and of the IR bands of silicic network at 1000 and 800 cm^{-1} (Figures 11 and 12)). This is also attested by the fact that the Ni loading in these samples (Table 1) is very close to that in bulk 1:1 nickel phyllosilicate ($Si_2Ni_3O_5(OH)_4$, 46 wt % Ni). Therefore, the deposition−precipitation beyond 16 h corresponds to an aging period. This is emphasized by the fact that the crystallinity of 1:1 nickel phyllosilicate increases between 16 and 100 h of DP, as attested by the XRD and TPR results (Figures 9, 10, 17, and 18).

Silica erosion is due to its dissolution in basic medium[59] and the subsequent or simultaneous reaction with nickel species to form 1:1 nickel phyllosilicate. Hence, silica is not an inert support but a true reactant, and deposition−precipitation cannot be considered as the mere precipitation of a Ni(II) phase on a support. The fact that the nature of the deposited−precipitated nickel depends on the silica surface area for short deposition−precipitation time indicates that the chemical mechanism of deposition−precipitation, which will be discussed in a forthcoming paper,[33] is not only related to the formation of 1:1 nickel phyllosilicate but results from a competition between the formation of nickel hydroxide and 1:1 nickel phyllosilicate. This competition is probably connected with the kinetics of silica dissolution, which is also dependent on the silica surface area.

The fact that the Ni loading in Ni/SiO_2 (≥16 h) samples corresponds to the deposition−precipitation of about 100% of the nickel (Table 1) also suggests that the amount of Ni(II) species eliminated during the washing step after deposition−precipitation is very low (see Experimental Section). This is confirmed by the presence of a small TPR peak of nickel carbonate when the sample is not previously washed (Figure 19a).

It may be also noted that (i) the Ni/Si atomic ratio in the initial suspension is equal to 1.1 while that in 1:1 nickel phyllosilicate is equal to 1.5 and that in 2:1 nickel phyllosilicate is equal to 0.75; (ii) the formation of 2:1 nickel phyllosilicate is thermodynamically favored (Table 8); (iii) only 1:1 nickel phyllosilicate is formed during deposition−precipitation, except when subsequent hydrothermal treatment is performed. These facts indicate that the Ni(II) deposition−precipitation on silica at 90 °C and atmospheric pressure is governed by kinetics and especially the kinetics of silica dissolution, and not by thermodynamics. The formation of a 2:1 nickel phyllosilicate involves the depolymerization of 1:1 nickel phyllosilicate formed first (kinetic compound), and the reprecipitation of 2:1 nickel phyllosilicate (i.e., the thermodynamic compound); this step is probably too slow at 90 °C and at amospheric pressure to lead to the formation of 2:1 nickel phyllosilicate in the conditions of deposition−precipitation.

Conclusion

This study on the characterization of the Ni/SiO_2 samples prepared by deposition−precipitation by urea hydrolysis has revealed that the nature of the deposited−precipitated nickel-(II) phase depends on the silica surface area and the deposition−precipitation time. For short DP time (≤4 h) and with silica of high surface area (≈400 $m^2 \cdot g^{-1}$), the deposited−precipitated Ni(II) phase is mainly an ill-crystallized 1:1 nickel phyllosilicate while with silica of low surface area (≈50 $m^2 \cdot g^{-1}$), the deposited−precipitated Ni(II) phase has been identified as mainly a turbostratic nickel hydroxide. For long DP time (>4 h) and both types of silica, the deposited−precipitated Ni(II) phase is a 1:1 nickel phyllosilicate. However, it is better crystallized with silica of low surface area. Almost the same Ni(II) phases are obtained whether silica is porous or not, with the difference that on nonporous silica of low surface area, and for short DP time, the Ni(II) phase is a mixture of 1:1 nickel phyllosilicate and nickel hydroxide. In addition, the deposited−precipitated Ni(II) phase is better crystallized and the interface with the support is larger with nonporous silica than with porous ones, because of the more regular shape of the silica particles.

Our results show that the mechanism of deposition−precipitation results from a competition between the formation of nickel hydroxide and that of 1:1 nickel phyllosilicate and that this mechanism is governed by the kinetics of silica dissolution, which acts as a true reactant. The whole mechanism is governed by kinetics and not by thermodynamics since only 1:1 nickel phyllosilicate, the kinetic compound, and not 2:1 nickel phyllosilicate, the thermodynamically stable compound, is formed in the conditions of deposition-precipitation.

Acknowledgment. The authors are indebted to Rhône Poulenc (France) for financial support of this work. They warmly thank Prof. A. Decarreau (HydrASA, URA 721 CNRS, Université de Poitiers, France) for helpful discussions and for the synthesis of bulk nickel phyllosilicates. They also warmly thank Dr. M. Kermarec (Laboratoire de Réactivité de Surface)

for helpful discussions on IR spectroscopy, as well as the student Véronique Thétiot for additional experiments.

References and Notes

(1) Houalla, M.; Delannay, F.; Matsuura, I.; Delmon, B. *J. Chem. Soc., Faraday Trans. 1* **1980**, *76*, 2128.
(2) Turlier, P.; Praliaud, H.; Moral, P.; Martin, G. A.; Dalmon, J. A. *Appl. Catal.* **1985**, *19*, 287.
(3) Mile, B.; Stirling, D.; Zammit, M. A.; Lovell, A.; Webb, M. *J. Catal.* **1988**, *114*, 217.
(4) Bonneviot, L.; Clause, O.; Che, M.; Manceau, A.; Dexpert, H. *Catal. Today* **1989**, *6*, 39.
(5) Clause, O.; Bonneviot, L.; Che, M.; Dexpert, H. *J. Catal.* **1991**, *130*, 21.
(6) Clause, O.; Kermarec, M.; Bonneviot, L.; Villain, F.; Che, M. *J. Am. Chem. Soc.* **1992**, *114*, 4709.
(7) Louis, C.; Cheng, Z. X.; Che, M. *J. Phys. Chem.* **1993**, *97*, 5703.
(8) Kermarec, M.; Carriat, J. Y.; Burattin, P.; Che, M.; Decarreau, A. *J. Phys. Chem.* **1994**, *98*, 12008.
(9) Okamoto, Y.; Nagata, K.; Adachi, T.; Imanaka, T.; Inamura, K.; Takyu, T. *J. Phys. Chem.* **1991**, *95*, 310.
(10) Clause, O. Ph.D. Thesis, Paris, 1989.
(11) Toupance, T.; Louis, C., unpublished results.
(12) Huong, L. L. Ph.D. Thesis, Paris, 1995.
(13) Pernot, H.; Kermarec, M., personal communication.
(14) Geus, J. W. Dutch Patent Applications, 1967, 6705, 259, and 1968, 6813, 236.
(15) van Dillen, J. A.; Geus, J. W.; Hermans, L. A.; van der Meijden, J. In *Proceedings of the 6th International Congress on Catalysis, London, 1976*; Bond, G. C.; Wells, P. B., Tompkins, F. C. Eds.; The Chemical Society: London, 1977; p 677.
(16) Hermans, L. A. M.; Geus, J. W. In *Preparation of Catalysts II*; Delmon, B.; Grange, P.; Jacobs, P. A., Poncelet, G. Eds.; Elsevier: Amsterdam, 1979; p 113.
(17) Feitknecht, W.; Berger, A. *Helv. Chim. Acta* **1942**, *25*, 1543.
(18) Longuet, J. *C. R. Acad. Sci. Paris* **1947**, *225*, 869.
(19) Franzen, P.; van Eijk van Voorthuysen, J. J. B. *Trans. 4th Int. Congr. Soil Sci., Amsterdam*, **1950**, p 34.
(20) Shaw, W. H. R.; Bordeaux, J. J. *J. Am. Chem. Soc.* **1955**, *77*, 4729.
(21) Coenen, J. W. E.; Schats, W. M. T. M.; van Meerten, R. Z. C. *Bull. Soc. Chim. Belg.* **1979**, *88*, 435.
(22) Coenen, J. W. E. *Appl. Catal.* **1989**, *54*, 65.
(23) Coenen, J. W. E. *Appl. Catal.* **1991**, *75*, 193.
(24) Montes, M.; Penneman de Bosscheyde, C.; Hodnett, B. K.; Delannay, F.; Grange, P.; Delmon, B. *Appl. Catal.* **1984**, *12*, 309.
(25) Gil, A.; Diaz, A.; Gandia, L. M.; Montes, M. *Appl. Catal. A* **1994**, *109*, 167.
(26) Richardson, J. T.; Dubus, R. T. *J. Catal.* **1978**, *54*, 207.
(27) Richardson, J. T.; Dubus, R. J.; Crump, J. G.; Desai, P.; Osterwalder, U.; Cale, T. S. In *Preparation of Catalysts II*; Delmon, B., Grange, P., Jacobs, P. A., Poncelet, G., Eds.; Elsevier: Amsterdam, 1979; p 131.
(28) Montes, M.; Soupart, J. B.; de Saedeleer, M.; Hodnett, B. K.; Delmon, B. *J. Chem. Soc., Faraday Trans. 1* **1984**, *80*, 3209.
(29) Blackmond, D. A.; Ko, E. I. *Appl. Catal.* **1984**, *13*, 49.
(30) Delmon, B. *J. Mol. Catal.* **1990**, *59*, 179.
(31) Keane, M. A. *Can. J. Chem.* **1994**, *72*, 372.
(32) Coenen, J. W. E. *Appl. Catal.* **1989**, *54*, 59.
(33) Burattin, P.; Che, M.; Louis, C., manuscript in preparation.
(34) Bailey, S. W. In *Crystal Structures of Clay Minerals and their X-ray Identification*; Brindley, G. W., Brown, G., Eds.; Mineralogical Society: London, 1980; p 1.
(35) Decarreau, A. *Bull. Miner.* **1980**, *103*, 579.
(36) Le Bihan, S.; Guenot, J.; Figlarz, M. *C. R. Acad. Sci. Paris* **1970**, *C270*, 2131.
(37) Génin, P.; Delahaye-Vidal, A.; Protemer, F.; Tekaia, F.; Figlarz, M. *Eur. J. Solid State Inorg. Chem.* **1991**, *28*, 505.
(38) Decarreau, A. *Geochim. Cosmochim. Acta* **1985**, *49*, 1537.
(39) Michalowicz, A. In *Logiciels pour la Chimie*; Société Française de Chimie: Paris, 1991; p 102.
(40) Figlarz, M.; Le Bihan, S. *C. R. Acad. Sci. Paris* **1971**, *C272*, 280.
(41) Foster, D.; Goodgame, D. M. L. *J. Chem. Soc.* **1965**, 262.
(42) Ellestad, O. H.; Klaeboe, P.; Tucker, E. E.; Songstad, J. *Acta Chem. Scand.* **1972**, *26*, 1724.
(43) Nakamoto, K. *Infrared and Raman Spectra of Inorganic and Coordination Compounds*; J. Wiley and Sons: New York, 1978.
(44) Mondésir, H. Ph.D. Thesis, Paris-Sud, 1987.
(45) Mondésir, H.; Decarreau, A. *Bull. Minéral.* **1987**, *110*, 409.
(46) Decarreau, A.; Mondésir, H.; Besson, G. *C. R. Acad. Sci. Paris (Sér. II)* **1989**, *308*, 301.
(47) Gérard, P.; Herbillon, A. J. *Clays Clay Miner.* **1983**, *31*, 143.
(48) Couty, R.; Decarreau, A.; Perruchot, A. *C. R. Acad. Sci. Paris (Sér. II)* **1981**, *292*, 1269.
(49) Lippincott, E. R.; van Valkenberg, A.; Weir, C. E.; Bunting, E. N. *J. Res. Natl. Bur. Stand.* **1958**, *A61*, 61.
(50) Decarreau, A., personal communication.
(51) Carriat, J. Y. Ph.D. Thesis, Paris, 1994.
(52) Carriat, J. Y.; Che, M.; Kermarec, M.; Decarreau, A. *Catal. Lett.* **1994**, *25*, 127.
(53) Geus, J. W. In *Preparation of Catalysts III*; Poncelet, G., Grange, P., Jacobs, P. A., Eds.; Elsevier: Amsterdam, 1983; p 1.
(54) Babu, G. P.; Basrur, A. G.; Bhat, A. N.; Murthy, R. S. *Ind. J. Chem.* **1990**, *29A*, 1094.
(55) Ghuge, K. D.; Bhat, A. N.; Babu, G. P. *Appl. Catal. A* **1993**, *103*, 183.
(56) Ghuge, K. D.; Babu, G. P. *J. Catal.* **1995**, *151*, 453.
(57) Smurov, A. A. *Mém. Soc. Russ. Minér.* **1938**, *67*, 465.
(58) Hénin, S.; Robichet, O. *C. R. Acad. Sci. Paris* **1954**, *238*, 2254.
(59) Iler, R. *The Chemistry of Silica*; J. Wiley and Sons: New York, 1979.
(60) Burattin, P. Ph.D. Thesis, Paris, 1994.
(61) de Roos, G.; Fluit, J. M.; Hermans, L. A. M.; Geus, J. W. *Z. Anorg. Allg. Chem.* **1979**, *449*, 115.
(62) Tardy, Y.; Garrels, R. M. *Geochim. Cosmochim. Acta* **1977**, *41*, 87.
(63) Sverjensky, D. A. *Geochim. Cosmochim. Acta* **1977**, *49*, 853.
(64) van Eijk van Voorthuysen, J. J. B.; Franzen, P. *Recl. Trav. Chim.* **1951**, *70*, 793.
(65) Martin, G. A.; Renouprez, A.; Dalmai-Imelik, G.; Imelik, B. *J. Chim. Phys.* **1970**, *67*, 1149.